

海南石碌铁矿独居石的成因类型、化学定年及地质意义^{*}

王智琳^{1,2} 许德如^{2**} MONIKA Agnieszka Kusiak³ 吴传军^{2,4} 于亮亮^{2,4}

WANG ZhiLin^{1, 2}, XU DeRu^{2**}, MONIKA Agnieszka Kusiak³, WU ChuanJun^{2, 4} and YU LiangLiang^{2, 4}

1. 中南大学地球科学与信息物理学院,有色金属成矿预测教育部重点实验室,长沙 410083

2. 中国科学院广州地球化学研究所,中国科学院矿物学与成矿学重点实验室,广州 510640

3. Institute of Geological Sciences, Polish Academy of Sciences, 00-818 Warszawa, Poland

4. 中国科学院大学,北京 100049

1. MOE Key Laboratory of Metallogenetic Prediction of Nonferrous Metals, School of Geosciences and Info-Physics, Central South University, Changsha 410083, China

2. CAS Key Laboratory of Mineralogy and Metallogeny, Guangzhou Institute of Geochemistry, Chinese Academy of Sciences, Guangzhou 510640, China

3. Institute of Geological Sciences, Polish Academy of Sciences, 00-818 Warszawa, Poland

4. University of Chinese Academy of Sciences, Beijing 100049, China

2014-02-17 收稿, 2014-04-04 改回.

Wang ZL, Xu DR, Monika AK, Wu CJ and Yu LL. 2015. Genesis of and CHIME dating on monazite in the Shilu iron ore deposit, Hainan Province of South China, and its geological implications. *Acta Petrologica Sinica*, 31(1):200–216

Abstract Shilu iron ore deposit in Hainan Province is the largest hematite-rich deposit in China, associated with cobalt, copper and other polymetallic mineral resources. This deposit is largely hosted within the Neoproterozoic Shilu Group, a suite of low-grade, neritic siliciclastic and carbonate sedimentary succession with generally greenschist (locally up to amphibolite) facies metamorphism. The NWW-trending synclinorium is main ore-controlling structure for iron, cobalt and copper ore bodies in the district. Previous studies suggested that folding and associated ductile shearing and high-temperature plastic flow had played an important role in enrichment of iron, cobalt and copper metals. To confirm this, we carried out in situ analysis on chemical compositions and CHIME (total Th-U-Pb) dating on monazite from the proximal diopside-tremolite rocks in the Shilu Group, using electronic probe microanalysis (EPMA) on thin sections assisted by BSE image. Microscopic observation revealed an alignment of monazite parallel to regional foliation defined by low amphibolite-facies minerals, and that monazite was characterized by typical replacement of breakdown coronas with obviously mineral concentric zoning, i. e., monazite in the core successively ringed by apatite, allanite and epidote towards rims. EPMA analysis suggests that monazite is composed of cerium phosphate ((Ce, La, Nd, Th)PO₄) with cheralite as the main end member. The typical occurrence, ThO₂ contents (ranging from 0.78% to 4.61%) and REE pattern all indicate a metamorphic origin for studied monazite. CHIME dating results show that monazite yields the apparent ages ranging from 397Ma to 614Ma with a main age peak at 455Ma and a subordinate peak at 564Ma. Low contents of ThO₂ (0.78% ~ 1.65%), PbO (0.02% ~ 0.04%) and CaO (0.50% ~ 0.97%), and high ratios of Th/U (23.06 ~ 53.11) could interpret monazite with ca. 564Ma age as production of the early deformational metamorphic event. Subsequent dissolution-reprecipitation of monazite, during the later shear deformation, caused patchy zonation and chemical alteration of crystallised monazite domains. This process finally reset the U-Th-Pb system by the aids of possible alkali-bearing metamorphic fluid, and yielded the main peak age of ca. 455Ma. The patchy domains have variable contents of ThO₂ (0.92% ~ 4.61%), PbO (0.01% ~ 0.08%) and CaO (0.28% ~ 1.58%), and high Th/U ratios (24.83 ~ 52.86). The breakdown of

* 本文受国家自然科学基金项目(41302049, 41472171)、国家“973”项目(2012CB416806)和中国科学院矿物学与成矿学重点实验室合作研究基金(KLMM20120102)资助。

第一作者简介: 王智琳,女,1984年生,博士后,矿物学专业,E-mail: wangzhilin1025@163.com

** 通讯作者:许德如,男,1966年生,博士、研究员,从事于大陆边缘构造与成矿学研究,E-mail: xuderu@gig.ac.cn

monazite to the coronal minerals was most likely related to the process of post-deformational greenschist-facies retrograde metamorphism with the participation of possible Ca-, Fe-, Si-, Al-rich fluids by unbalance reaction. The reactive mechanism is elemental diffusion between monazite and coronas minerals, indicating that the REE, Y, and Th were mobile at a small scale and partial Pb loss may have happened in the rim of monazite. In line with the tectonic development of south China, we suggested that the ca. 455 Ma age likely recorded a regionally metamorphic event corresponding to South China Caledonian orogeny. Whereas the 564 Ma age might be linked to Pan-African event, implying that South China had an affinity to Gondwanaland in late Neoproterozoic to early paleozoic. Based on the available age data, the Caledonian event in South China could be considered as the subsequently intracontinental orogeny corresponding to the assembly and collision of Gondwanaland. Therefore, the Late Neoproterozoic to Early Paleozoic orogenic events might play an important role on the tectonic evolution of Hainan Island. Moreover, the orogenic event (s) had great significance for the enrichment of iron, cobalt and copper metals in the Shilu deposit.

Key words Monazite; Breakdown coronas; CHIME dating; Caledonian orogeny; Gondwanaland; Shilu iron ore deposit in Hainan Province

摘要 海南石碌铁矿是我国最大的富赤铁矿矿床,同时伴生有钴、铜等多金属矿产。轴向北西-南东向的复式向斜是石碌铁、钴铜矿体的主要控矿构造,富铁矿和钴铜矿的形成与该褶皱变形及伴随的韧性剪切和高温塑性流动有着密切的关系。为获得该构造变形的年代学信息和证实构造变形对成矿物质的富集影响,本文开展了石碌铁矿近矿围岩—石碌群第六层透辉石透闪石岩中独居石的显微结构观察和电子探针化学Th-U-Pb定年(CHIME法)。显微结构观察发现独居石往往沿岩石面理定向分布,且具典型的球冠结构,表现为围绕独居石核部向外依次出现磷灰石、褐帘石、绿帘石同心环。电子探针分析结果表明这些独居石为Ce-La-Nd磷酸盐[(Ce, La, Nd, Th)PO₄],具富钍独居石端元组分。ThO₂含量范围(0.78%~4.61%)、稀土特征以及独居石的产出特征均暗示了其为同构造变质成因。电子探针CHIME化学定年结果表明独居石的年龄变化范围为614~397 Ma,并具有两个峰值年龄:即主峰值ca. 455 Ma和次峰值ca. 564 Ma。低的ThO₂(0.78%~1.65%), PbO(0.02%~0.04%)和CaO(0.50%~0.97%)含量,以及高的Th/U比值(23.06~53.11)暗示了构成ca. 564 Ma的独居石是早期剪切变形事件的产物。而在随后剪切变形过程中独居石在低角闪岩相变质条件下以及碱性变质流体诱导下发生了溶解-再沉淀,形成了具ca. 455 Ma年龄的补丁状成分区。该过程引起了U-Pb体系的局部重置,形成的独居石具有变化较大的ThO₂(0.92%~4.61%)、PbO(0.01%~0.08%)和CaO(0.28%~1.58%)含量范围以及Th/U值(24.83~52.86)。在剪切变形之后,早期变质成因的独居石在绿片岩相退变质作用过程中及富Ca/Fe/Si/Al流体参与的条件下,经不平衡反应形成了磷灰石-褐帘石-绿帘石球冠物,反应机制以独居石和球冠矿物间的元素扩散动力学为主。该反应暗示了REE、Y、Th等元素发生了迁移,并可能引起边部独居石的部分Pb丢失。结合华南的构造演化,年龄谱主峰值455 Ma代表了与华南加里东造山运动有关的区域变质和动力变质作用事件年龄,是加里东运动在海南岛的响应;次峰值年龄564 Ma对应着冈瓦纳泛非事件,暗示了华南在晚新元古代-早古生代与冈瓦纳大陆具有亲缘性,华南加里东运动引起陆内造山过程可能与冈瓦纳大陆的聚合碰撞事件有关。因此,晚新元古代-早古生代造山事件对海南岛构造演化历史具重要影响。此外,该构造运动使石碌群发生褶皱变形,伴随产生的变质流体使铁、钴铜成矿元素进一步活化和富集,对石碌铁、钴铜矿的富集有着重要影响。

关键词 独居石;球冠结构;CHIME年定;华南加里东运动;冈瓦纳大陆;海南石碌铁矿

中图法分类号 P578.92; P597.3

独居石[(LREE, Th)PO₄]是变质岩中常见的副矿物,可形成于进变质和退变质过程各个阶段(Finger *et al.*, 1998; 王汝成等, 2006; Williams *et al.*, 2007; Zhu *et al.*, 1997a, b)。该矿物以富轻稀土为特征,具有高的U/Th和低的普通铅含量,因而被广泛用于Th-U-Pb定年,以重塑(多相)变质地体的构造历史、造山过程及变质或热液交代事件(Lanzirotti and Hanson, 1996; Suzuki and Adachi, 1998; Chen *et al.*, 2006, 2011; 王汝成等, 2006; Williams *et al.*, 2007)。电子探针Th-U-Pb化学定年(即CHIME法:Suzuki *et al.*, 1991; Montel *et al.*, 1996)具有高空间分辨率(分析束斑<5 μm),通过该方法可获得与不同热-构造变质事件对应的成分均匀区域的化学年龄。结合其原位分析的优势,可合理地解释年龄结果所代表的地质意义(刘树文等, 2004)。

海南岛位于欧亚板块、太平洋板块和印度-澳大利亚板块结合部位,这一独特的大地构造位置使其成为研究华南及

其与特提斯洋的演化和冈瓦纳大陆,以及Rodinia超大陆聚合和裂解的理想对象(Li *et al.*, 2002a, b, 2008a, b; Metcalfe, 1996; Xu *et al.*, 2007)。国内不同科研和生产部门先后在海南岛开展了大量的基础地质研究和找矿工作,并取得了一系列进展(侯威等, 1996; 汪啸风等, 1991a, b, c; 许德如等, 2003; 张业明等, 1998; 中国科学院华南富铁科学研究队, 1986)。然而,由于植被覆盖广,露头条件差,且构造和岩浆活动强烈,岛内地层多遭受严重破坏和强烈变形变质,相关构造运动及其性质的研究程度低,特别是加里东运动(或称为广西运动)在海南岛是否存在及其响应特征这一重要基础地质问题还存在争议,如:海南岛是否存在泥盆系地层、是否有加里东期花岗岩(付建明和赵子杰, 1997; 汪啸风等, 1991a, b, c; 张业明等, 1998; Zhang *et al.*, 2001)。此外,关于海南岛重要的矿产资源——石碌铁矿的成矿时代也存在着不同的认识,或根据生物群化石和铁矿石的Sm-Nd

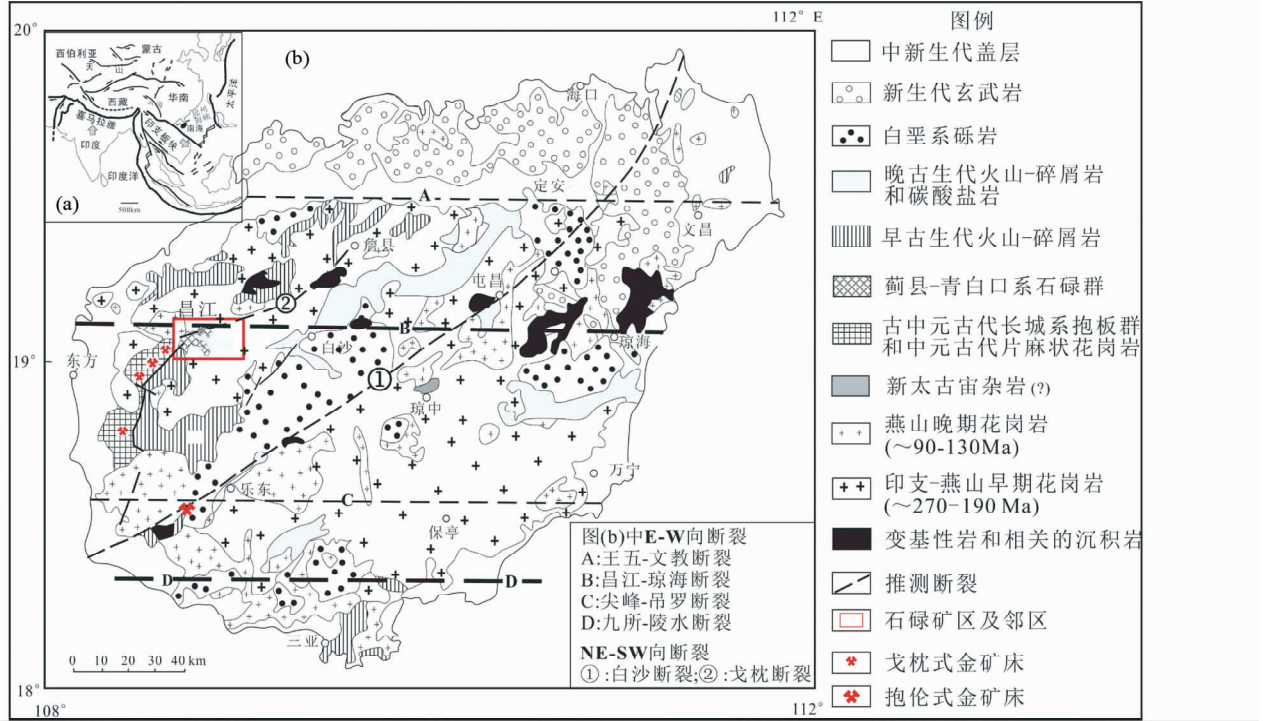


图1 海南岛区域地质和矿产简图(据 Xu et al., 2013 修改)

Fig. 1 Simplified regional geological and mineral resource map of Hainan Island (modified after Xu et al., 2013)

同位素年龄认为沉积铁矿形成于青白口纪(Zhang et al., 1990; 张仁杰等, 1992), 或根据构造变形、变质作用以及岩浆热液活动特征认为成矿作用过程具有多阶段性(Xu et al., 2013; 陈国达等, 1977; 侯威等, 1996, 2007; 许德如等, 2009; 张业明等, 1998), 而铁矿的富集被认为与石碌群的褶皱变形及伴随的剪切和高温塑性流动有着密切关系(Xu et al., 2013), 但关于各阶段的成矿时间一直缺乏直接的同位素年代学证据。因此石碌铁矿床的成矿时代急需有效的同位素年代学制约。本文在对石碌铁矿的近矿围岩、即石碌第六层透辉石透闪石岩中独居石进行显微结构观察的基础上, 开展了 CHIME 化学定年, 目的在于获得近矿围岩的变形变质年龄, 不仅为深入研究石碌群构造变形的动力学机制、而且为进一步探索华南加里东运动在海南岛的可能响应及华南(包括海南岛)在冈瓦纳聚合过程中的可能位置提供年代学证据。

1 地质背景

海南岛以琼州海峡与华南大陆相隔, 是我国东南陆缘海域中最大的岛屿, 该特殊的大地构造位置使其受太平洋和特提斯两大构造域的联合控制, 因而具有复杂的地质构造演化历史。海南岛构造形迹多样, 主要呈近东西向和北东向, 其次为北西向(图1), 这些构造形迹控制了海南岛不同时期的沉积建造、变质建造、岩浆建造和成矿作用事件。除泥盆系

和侏罗系地层尚无可靠证据外, 海南岛地层发育较全, 主要出露有古生界地层, 其次是元古宇和中新生界。其中元古宇地层主要出露于海南岛西部, 包括中元古界抱板群(约 1800 ~ 1450 Ma)和中-新元古界石碌群及上覆的震旦系石灰顶组(Xu et al., 2013)。海西-印支期(270 ~ 190 Ma)和燕山期花岗岩(130 ~ 90 Ma)是岛内主要的岩浆类型(Li et al., 2006; 葛小月, 2003), 出露面积约占全岛的 60%。不同时代的喷出岩在海南岛均有出现, 占全岛面积的 13% (汪啸风等, 1991a, b, c), 时代以中、新生代为主, 主要分布于琼北和岛南地区(图1)。

石碌铁矿位于近 EW 向昌江-琼海深大断裂和 NE 向戈枕韧-脆性断裂交汇部位的东南侧(图 1b)。矿区主要控矿构造为一轴向北西-南东向的复式向斜(图 2), 该复式向斜向西扬起、收敛, 向东南倾伏开阔, 自北而南, 依次由北一向斜、红房山背斜和石灰顶向斜等次级褶皱组成, 铁矿体、钴铜矿体多赋存在该复式向斜槽部及两翼向槽部过渡的部位。矿区出露的地层主要有中-新元古界石碌群、震旦系石灰顶组、石炭系南好组-青天峡组、二叠系峨查组-峨顶组和南龙组。其中, 石碌群是铁、钴铜矿的主要赋矿地层, 系一套以绿片岩相变质为主(局部达角闪岩相)的浅海、浅海-泻湖相的(火山?)碎屑沉积岩和碳酸盐岩建造。自下而上可分为六层: 第一、三、四、五层主要由石英云母片岩、云母石英片岩、石英岩和千枚岩等组成; 第二层主要由结晶白云岩、透辉石透闪石化的白云岩、白云质灰岩等组成。第六层是铁、钴铜矿的主要赋矿层位, 可分为三段: 上段主要由白云岩、含泥质或炭质

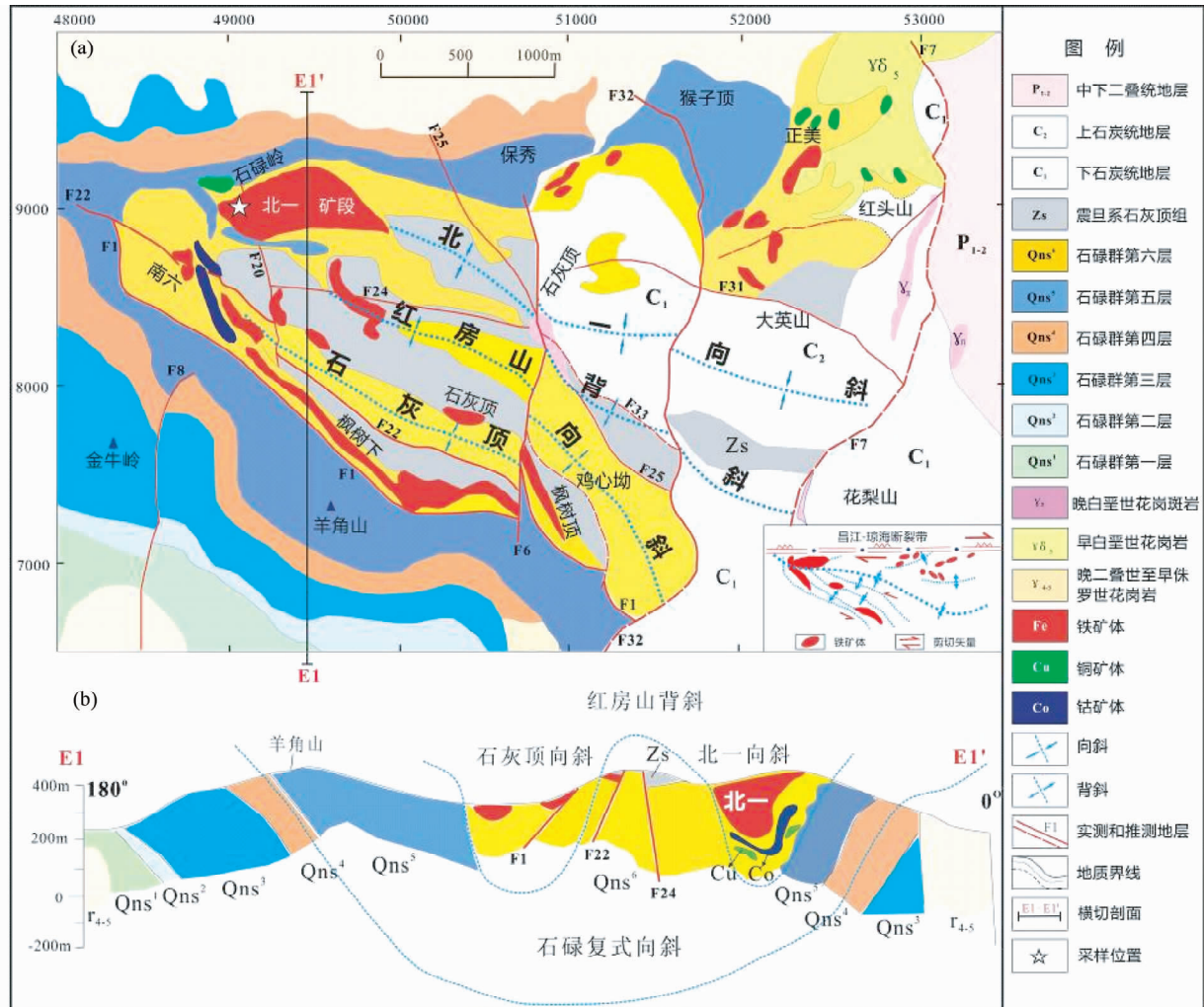


图2 海南石碌铁矿矿区地质简图(据 Xu et al. , 2013 修改)

Fig. 2 Simplified geological map of the Shilu iron ore mining, Hainan Island (modified after Xu et al. , 2013)

白云岩、灰岩及白云质灰岩组成, 夹炭质板岩或千枚岩, 含 *Churia-Tawuia*(宏观藻类)化石 (Zhang et al. , 1990), 残余沉积结构发育; 中段是含铁的主要层位, 由条带状透辉石透闪石岩、含石榴子石眼球或条带的透辉石透闪石岩、条带状白云岩及铁质千枚岩或铁质砂岩组成, 局部夹重晶石、石膏和碧玉层, 该段夹多层赤铁矿层; 下段是重要的含钴铜矿层位, 以条带状白云岩、白云岩和条带状透辉石透闪石岩为主, 夹硅质岩、石英绢云母片岩等。矿区及周缘侵入岩发育, 主要为印支-燕山期花岗岩 (葛小月, 2003; 侯威等, 1996)。矿区内尚发育有花岗斑岩、闪长玢岩、煌斑岩、辉绿岩等燕山晚期岩脉 (侯威等, 1996; 王智琳等, 2011)。

2 样品描述和独居石的产出状态

所分析的透辉石透闪石岩样品 F8-7 采自石碌矿区北一钴铜矿段, 是钴铜矿体的直接赋矿围岩。岩石呈灰白色-灰

绿色, 主要由透闪石、阳起石、透辉石、钾长石、石英、黑云母及少量的绿帘石等组成, 副矿物有磷灰石、榍石、锆石、独居石等。岩石结构以粒状变晶结构、纤状变晶结构、鳞片变晶结构为主, 构造以互层的钾长石 + 石英、透辉石 ± 透闪石和/或透闪石 + 阳起石 + 钾长石组成的条纹条带状构造为特征 (图 3a, b)。

独居石主要以包裹体的形式产出在变质矿物如钾长石、黑云母中 (图 4), 粒径约 $10 \sim 30 \mu\text{m}$, 多为长条形或米粒状, 少量独居石颗粒呈不规则状, 甚至为不连续的碎片 (见后文)。由 BSE 图像可知, 少量独居石具有成分不均一区, 这可能与 Th 的含量变化 (Janots et al. , 2012)。岩相学观察发现部分独居石显示典型的分解球冠结构 (monazite breakdown coronas), 即围绕独居石组成的核依次出现磷灰石、褐帘石、绿帘石矿物集合体同心环带 (图 4c-f)。磷灰石除普遍围绕独居石呈集合体环带分布外, 部分磷灰石中还可见亮的钛石斑点 (图 4e)。磷灰石和独居石的接触界线多为港湾状, 但若独居石裂隙或解理发育, 则磷灰石优先沿裂隙或解理面分

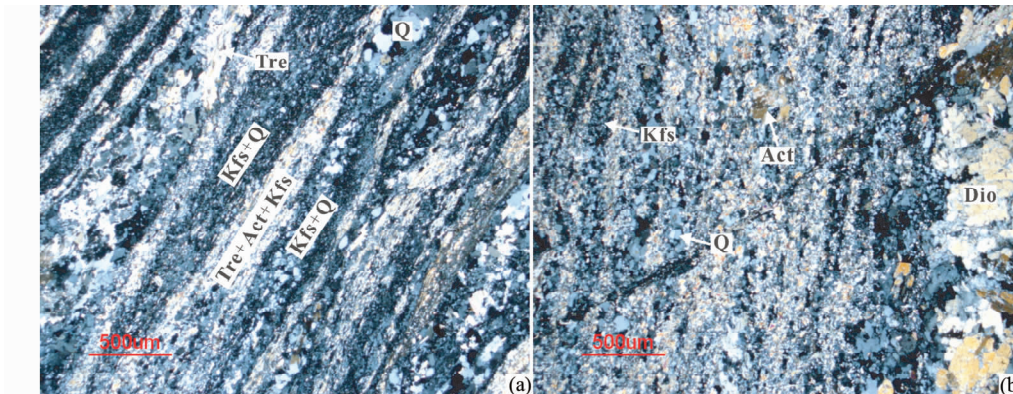


图3 海南石碌矿区条带状透辉石透闪石岩的显微组构特征

(a)由互层的钾长石+石英与透闪石+阳起石+钾长石组成的条纹条带状构造,正交偏光;(b)粒状变晶结构的透辉石集合体组成的条带与透闪石+阳起石+钾长石组成的条带互层,正交偏光. Kfs-钾长石;Q-石英;Tre-透闪石;Act-阳起石;Dio-透辉石

Fig. 3 Microstructure of the banded diopside-tremolite rock in the Shilu mining area, Hainan Island

(a) the banded structure composed by K-feldspar + quartz alternating with tremolite + actinolite + K-feldspar, doubly polarized light; (b) microbanding of aggregates of diopside with granoblastic texture and tremolite + actinolite + K-feldspar laminae, doubly polarized light. Kfs-K-feldspar; Q-quartz; Tre-tremolite; Act-actinolite; Dio-diopside

布(图4e),使得独居石被交代呈不规则状、乃至碎片状。此外,还可见少量独居石呈残留点状分布在磷灰石核部,这些现象均说明磷灰石是直接交代独居石形成的。褐帘石多呈他形,其边缘往往呈钉状或叶状凸向绿帘石。球冠结构最边部的绿帘石往往呈半自形-他形,其分布范围明显大于褐帘石。该球冠结构可能与独居石的分解反应有关(Finger *et al.*, 1998)。

3 分析方法

独居石 CHIME 化学定年采取在抛光良好的薄片上直接测定的方法。由于具放射性,独居石会在寄主矿物中形成放射性晕圈,由此可在薄片中快速找到独居石,也可根据独居石在电子探针背散射图像中为高亮白色来寻找。本文利用高对比度的背散射图像和 X 射线图像,选择颗粒较大且表面平整、没有裂隙和包体的独居石核部位置进行测点分析。测试分析是在斯洛伐克首都布拉迪斯拉法 State Geological Institute of Dionyz Stur 电子探针实验室完成,仪器为 Cameca SX-100 电子探针,装有四通道波谱仪和 KEVEX 能谱仪。实验条件为:加速电压 15kV,电流 180nA,电子束直径 2~3μm,相关元素分析所采用的计数时间、标样和检测限等条件见表 1。具体实验分析方法、数据处理和校正及年龄计算见(Petrík and Konečny, 2009)。

4 独居石电子探针分析结果

4.1 独居石成分结果

样品 F8-7 共分析了 17 个独居石颗粒,测点数 23 个,结果见表 2。由表 2 可知,La、Ce、Nd 占总阳离子数(除 P、Si、S

表 1 独居石电子探针分析的实验条件

Table 1 The analytical conditions of electron microprobe for monazite

元素	检测线	晶体	计数时间 (s)	检测限 ($\times 10^{-6}$)	标样
La	L α	LLIF	10	721	LaPO ₄
Ce	L α	LLIF	10	557	CePO ₄
Pr	L β	LLIF	30	625	PrPO ₄
Nd	L α	LLIF	10	568	NdPO ₄
Sm	L α	LLIF	10	858	SmPO ₄
Eu	L β	LLIF	30	781	EuPO ₄
Gd	L α	LLIF	20	386	GdPO ₄
Tb	L α	LLIF	15	633	TbPO ₄
Dy	L β	LLIF	50	729	DyPO ₄
Ho	L β	LLIF	60	574	HoPO ₄
Er	L β	LLIF	50	849	ErPO ₄
Tm	L α	LLIF	30	507	TmPO ₄
Yb	L α	LLIF	30	548	YbPO ₄
Lu	L β	LLIF	100	974	YbPO ₄
Pb	M α	LPET	300	91	PbCO ₃
U	M β	LPET	80	208	UO ₂
Th	M α	LPET	35	222	ThO ₂
P	K α	LPET	10	125	磷灰石
Fe	K α	LPET	20	222	铁橄榄石
S	K α	LPET	10	111	Pyrite
Sr	K α	LPET	20	356	SrTiO ₂
Al	K α	LPET	10	139	Al ₂ O ₃
As	L α	LPET	120	121	GaAs
Ca	K α	LPET	10	112	磷灰石
Y	L α	LPET	40	198	YPO ₄
Si	K α	TAP	10	132	SiO ₂

外)的 66%~89%,独居石的成分主要为 Ce-La-Nd 磷酸盐 [(Ce, La, Nd, Th)PO₄]。样品中 ThO₂ 含量变化范围为

表2 独居石的电子探针分析结果(wt%)

Table 2 The chemical composition for monazites by EPMA (wt%)

测点	1	2	3	4	5	6	7/1	7/2	8	9	10	11	12/1	12/2	13	14/1	14/2	15/1	15/2	15/3	16	17/1	17/2
SO ₃	0.48	0.36	0.25	0.47	0.62	0.43	0.23	0.17	0.10	0.27	0.37	0.20	0.34	0.40	0.29	0.58	0.29	0.36	0.26	0.37	0.30	0.57	0.67
P ₂ O ₅	28.11	30.23	26.21	29.49	29.62	29.03	29.61	29.08	29.21	29.05	28.87	28.75	28.95	28.44	28.22	28.57	27.81	28.97	28.87	28.38	28.94	28.55	28.87
As ₂ O ₅	0.16	0.17	0.15	0.16	0.19	0.21	0.15	0.16	0.13	0.15	0.14	0.16	0.14	0.17	0.19	0.17	0.21	0.15	0.15	0.18	0.16	0.18	0.16
SiO ₂	0.46	0.35	5.08	0.30	0.27	0.38	0.20	0.48	0.40	0.35	0.21	0.33	0.24	0.41	0.53	0.19	0.85	0.15	0.20	0.30	0.26	0.33	0.14
ThO ₂	2.05	1.65	1.35	2.74	2.28	2.21	0.78	3.04	1.57	2.58	1.60	2.77	1.23	3.98	4.37	0.92	4.61	0.92	1.21	2.19	2.05	4.05	1.24
UO ₂	0.02	0.04	0.04	0.02	0.02	0.02	0.01	0.01	0.01	0.01	0.01	0.01	0.01	0.01	0.01	0.01	0.01	0.01	0.02	0.02	0.04	0.03	0.02
Al ₂ O ₃	0.09	0.01	1.74	0.00	0.00	0.01	0.06	0.02	0.03	0.00	0.00	0.00	0.00	0.00	0.03	0.00	0.00	0.00	0.00	0.00	0.03	0.00	0.00
Y ₂ O ₃	0.39	0.57	0.22	0.50	0.88	0.75	0.19	0.36	0.29	0.49	0.34	0.37	0.26	0.56	0.52	0.35	0.43	0.41	0.39	0.49	0.42	0.53	0.28
La ₂ O ₃	13.18	8.91	12.88	10.71	6.03	6.68	21.77	14.53	18.47	14.68	15.88	15.48	16.49	9.41	7.56	11.59	6.73	17.73	16.69	13.01	17.01	7.42	15.88
Ce ₂ O ₃	32.18	28.58	30.71	31.64	25.23	26.25	32.66	32.34	32.70	32.31	32.64	32.21	33.28	30.09	28.07	33.13	24.77	32.64	33.11	32.13	32.35	28.26	33.50
Pr ₂ O ₃	3.63	4.11	3.13	4.08	4.24	4.34	2.98	3.54	3.26	3.52	3.42	3.47	3.42	4.07	4.08	4.06	4.10	3.38	3.42	3.66	3.36	4.18	3.49
Nd ₂ O ₃	13.36	18.38	10.13	15.56	21.17	21.51	9.57	12.61	11.09	12.65	12.33	12.25	11.55	16.12	17.50	15.27	20.60	11.62	11.91	13.80	11.55	18.25	11.79
Sm ₂ O ₃	1.87	3.65	1.24	2.38	5.21	5.26	1.03	1.64	1.37	1.60	1.68	1.50	1.43	2.72	3.26	2.19	4.66	1.35	1.45	1.90	1.27	3.46	1.42
Eu ₂ O ₃	0.20	0.49	0.19	0.31	0.67	0.52	0.16	0.24	0.18	0.18	0.22	0.21	0.22	0.38	0.38	0.24	0.41	0.17	0.18	0.31	0.19	0.36	0.20
Gd ₂ O ₃	0.85	1.94	0.00	1.10	2.54	2.19	0.19	0.66	0.54	0.71	0.62	0.61	0.46	1.27	1.43	0.86	1.60	0.49	0.47	0.77	0.46	1.41	0.41
Tb ₂ O ₃	0.03	0.12	0.03	0.05	0.07	0.03	0.00	0.01	0.02	0.06	0.04	0.05	0.08	0.10	0.06	0.03	0.05	0.03	0.05	0.02	0.02	0.05	0.02
Dy ₂ O ₃	0.19	0.34	0.08	0.22	0.45	0.40	0.09	0.14	0.16	0.29	0.16	0.23	0.15	0.25	0.28	0.19	0.28	0.21	0.17	0.25	0.21	0.31	0.13
Ho ₂ O ₃	0.00	0.00	0.00	0.03	0.02	0.01	0.00	0.00	0.01	0.00	0.00	0.00	0.03	0.01	0.05	0.04	0.00	0.03	0.00	0.00	0.03	0.02	
Er ₂ O ₃	0.24	0.28	0.32	0.33	0.30	0.31	0.31	0.34	0.30	0.31	0.27	0.33	0.33	0.34	0.26	0.36	0.31	0.34	0.34	0.33	0.27	0.33	
Tm ₂ O ₃	0.04	0.00	0.00	0.00	0.15	0.08	0.06	0.07	0.08	0.03	0.07	0.06	0.09	0.05	0.06	0.06	0.05	0.06	0.07	0.04	0.07	0.03	
Yb ₂ O ₃	0.09	0.18	0.13	0.06	0.11	0.13	0.11	0.10	0.10	0.11	0.12	0.11	0.11	0.14	0.13	0.09	0.13	0.09	0.11	0.09	0.06	0.11	
Lu ₂ O ₃	0.13	0.10	0.04	0.10	0.07	0.11	0.17	0.11	0.10	0.08	0.05	0.25	0.17	0.10	0.12	0.09	0.10	0.11	0.05	0.10	0.06	0.11	0.06
CaO	0.93	0.97	4.87	1.06	1.23	1.16	0.50	0.76	0.28	0.80	0.67	1.51	0.79	1.14	1.19	0.73	1.58	0.59	0.58	0.90	0.64	1.23	0.86
FeO	0.00	0.00	0.63	0.00	0.00	0.00	0.00	0.00	0.00	0.00	0.00	0.00	0.00	0.00	0.00	0.00	0.00	0.00	0.00	0.00	0.00	0.00	
SrO	0.07	0.08	0.05	0.05	0.08	0.05	0.04	0.05	0.04	0.04	0.06	0.03	0.04	0.08	0.04	0.05	0.04	0.05	0.04	0.02	0.05	0.06	0.10
PbO	0.03	0.04	0.03	0.05	0.04	0.04	0.02	0.06	0.03	0.05	0.03	0.05	0.02	0.07	0.08	0.01	0.06	0.02	0.03	0.04	0.04	0.08	0.03
Total	98.79	101.53	99.48	101.39	101.49	102.11	100.92	100.50	100.52	100.40	99.82	100.94	99.77	100.35	98.76	99.73	99.83	99.75	99.38	99.88	99.83	99.76	

续表2
Continued Table 2

阳离子数:基于24个氧原子	测点	1	2	3	4	5	6	7/1	7/2	8	9	10	11	12/1	12/2	13	14/1	14/2	15/1	15/2	15/3	16	17/1	17/2
S	0.087	0.061	0.041	0.081	0.108	0.075	0.041	0.031	0.018	0.048	0.066	0.035	0.061	0.072	0.052	0.103	0.053	0.064	0.046	0.066	0.053	0.101	0.119	
P	5.705	5.886	4.923	5.801	5.803	5.730	5.854	5.803	5.835	5.801	5.741	5.805	5.721	5.749	5.641	5.813	5.749	5.806	5.741	5.770				
As	0.020	0.021	0.017	0.020	0.023	0.025	0.018	0.019	0.017	0.018	0.018	0.020	0.018	0.021	0.024	0.021	0.027	0.018	0.019	0.022	0.020	0.022	0.019	
Si	0.109	0.080	1.126	0.070	0.062	0.088	0.047	0.113	0.094	0.083	0.050	0.077	0.056	0.097	0.127	0.046	0.204	0.035	0.048	0.071	0.062	0.080	0.034	
Th	0.112	0.086	0.068	0.145	0.120	0.117	0.042	0.163	0.084	0.139	0.086	0.149	0.066	0.215	0.239	0.050	0.251	0.049	0.066	0.119	0.110	0.219	0.067	
U	0.001	0.002	0.002	0.001	0.001	0.001	0.001	0.001	0.002	0.002	0.003	0.001	0.001	0.002	0.001	0.002	0.002	0.000	0.000	0.001	0.002	0.002	0.001	
Al	0.026	0.002	0.455	0.000	0.000	0.004	0.017	0.007	0.009	0.001	0.000	0.001	0.001	0.000	0.009	0.000	0.000	0.000	0.000	0.000	0.010	0.001	0.000	
Y	0.050	0.069	0.026	0.062	0.108	0.093	0.024	0.046	0.037	0.062	0.043	0.047	0.033	0.070	0.067	0.044	0.054	0.052	0.049	0.063	0.053	0.066	0.035	
La	1.166	0.756	1.054	0.918	0.515	0.574	1.875	1.263	1.607	1.277	1.390	1.347	1.441	0.824	0.671	1.016	0.595	1.550	1.464	1.148	1.487	0.651	1.383	
Ge	2.825	2.407	2.494	2.692	2.240	2.792	2.791	2.825	2.790	2.836	2.782	2.887	2.617	2.473	2.883	2.173	2.832	2.883	2.815	2.807	2.457	2.895		
Pr	0.318	0.344	0.253	0.346	0.358	0.369	0.254	0.304	0.281	0.303	0.296	0.298	0.296	0.353	0.358	0.352	0.358	0.292	0.296	0.319	0.290	0.362	0.300	
Nd	1.144	1.510	0.803	1.292	1.750	1.791	0.798	1.062	0.935	1.066	1.045	1.032	0.977	1.368	1.504	1.296	1.763	0.984	1.011	1.179	0.978	1.548	0.994	
Sm	0.155	0.290	0.095	0.191	0.416	0.423	0.083	0.133	0.112	0.130	0.138	0.122	0.117	0.223	0.271	0.179	0.386	0.110	0.119	0.157	0.104	0.283	0.115	
Eu	0.016	0.038	0.015	0.024	0.053	0.041	0.012	0.019	0.015	0.015	0.018	0.017	0.018	0.031	0.031	0.019	0.034	0.014	0.015	0.025	0.015	0.029	0.016	
Gd	0.067	0.148	0.000	0.085	0.195	0.169	0.015	0.051	0.042	0.055	0.049	0.048	0.036	0.100	0.114	0.068	0.127	0.038	0.037	0.061	0.036	0.111	0.032	
Tb	0.003	0.009	0.002	0.004	0.005	0.003	0.000	0.001	0.001	0.004	0.003	0.004	0.006	0.008	0.005	0.003	0.004	0.002	0.002	0.004	0.001	0.004	0.001	
Dy	0.015	0.025	0.005	0.017	0.034	0.030	0.007	0.010	0.012	0.022	0.012	0.017	0.011	0.019	0.021	0.015	0.022	0.016	0.013	0.020	0.016	0.024	0.010	
Ho	0.000	0.000	0.000	0.000	0.002	0.001	0.001	0.000	0.000	0.001	0.000	0.000	0.000	0.002	0.000	0.004	0.003	0.000	0.002	0.000	0.000	0.002	0.001	
Er	0.018	0.020	0.022	0.024	0.022	0.023	0.023	0.025	0.022	0.023	0.020	0.025	0.024	0.026	0.019	0.027	0.023	0.025	0.026	0.025	0.020	0.024		
Tm	0.003	0.000	0.000	0.000	0.010	0.005	0.004	0.005	0.005	0.006	0.002	0.005	0.004	0.006	0.003	0.005	0.004	0.004	0.004	0.006	0.003	0.005	0.002	
Yb	0.007	0.013	0.009	0.004	0.008	0.010	0.008	0.007	0.007	0.008	0.009	0.008	0.008	0.008	0.010	0.010	0.006	0.009	0.007	0.008	0.007	0.004	0.008	0.008
Lu	0.009	0.007	0.003	0.007	0.005	0.008	0.012	0.008	0.007	0.005	0.004	0.018	0.012	0.007	0.009	0.007	0.008	0.003	0.007	0.004	0.008	0.004	0.008	0.004
Ca	0.239	0.249	1.157	0.263	0.306	0.289	0.124	0.192	0.072	0.201	0.169	0.380	0.200	0.290	0.307	0.186	0.406	0.151	0.148	0.230	0.161	0.312	0.218	
Fe	0.000	0.000	0.117	0.000	0.000	0.000	0.000	0.000	0.000	0.000	0.000	0.000	0.000	0.000	0.000	0.000	0.000	0.000	0.000	0.000	0.000	0.000	0.000	
Sr	0.009	0.011	0.007	0.007	0.010	0.007	0.005	0.007	0.006	0.005	0.008	0.004	0.006	0.011	0.006	0.007	0.005	0.007	0.006	0.003	0.007	0.008	0.014	
Pb	0.002	0.002	0.002	0.003	0.002	0.002	0.001	0.004	0.002	0.003	0.002	0.003	0.001	0.005	0.005	0.001	0.004	0.001	0.002	0.002	0.003	0.005	0.002	
Total	12.11	12.03	12.69	12.06	12.05	12.12	12.06	12.05	12.07	12.07	12.18	12.09	12.10	12.08	12.08	12.16	12.07	12.07	12.10	12.06	12.07	12.07		

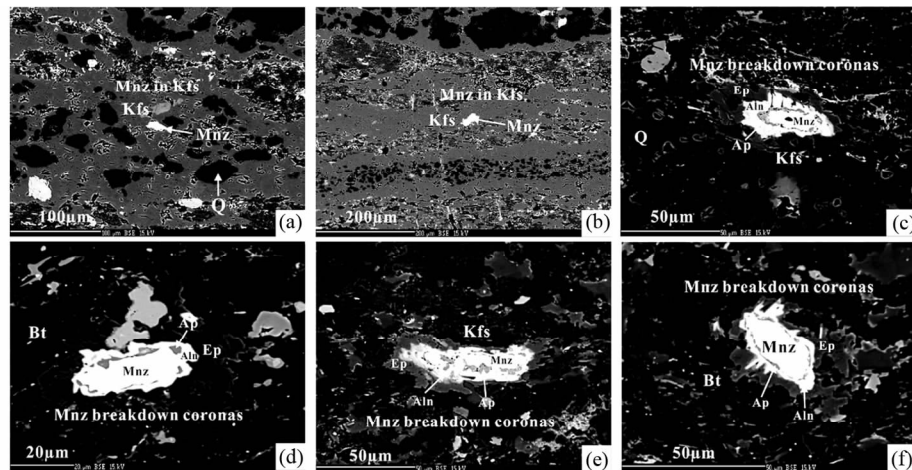


图4 电子探针背散射图像下的独居石显微特征

(a,b) 产出在钾长石+石英条带中的独居石颗粒; (c-f) 从边部到核部依次由绿帘石、褐帘石和磷灰石矿物环带组成的独居石球冠结构。Bt-黑云母; Mnz-独居石; Ap-磷灰石; Aln-褐帘石; Ep-绿帘石

Fig. 4 The microscopic characteristics of monazites in back-scatter electron images

(a, b) monazite grains in microbanding composed of K-feldspar + quartz; (c-f) monazite breakdown coronas comprising mineral zones of epidote, allanite and apatite successively from rim to core. Bt-biotite; Mnz-monazite; Ap-apatite; Aln-allanite; Ep-epidote

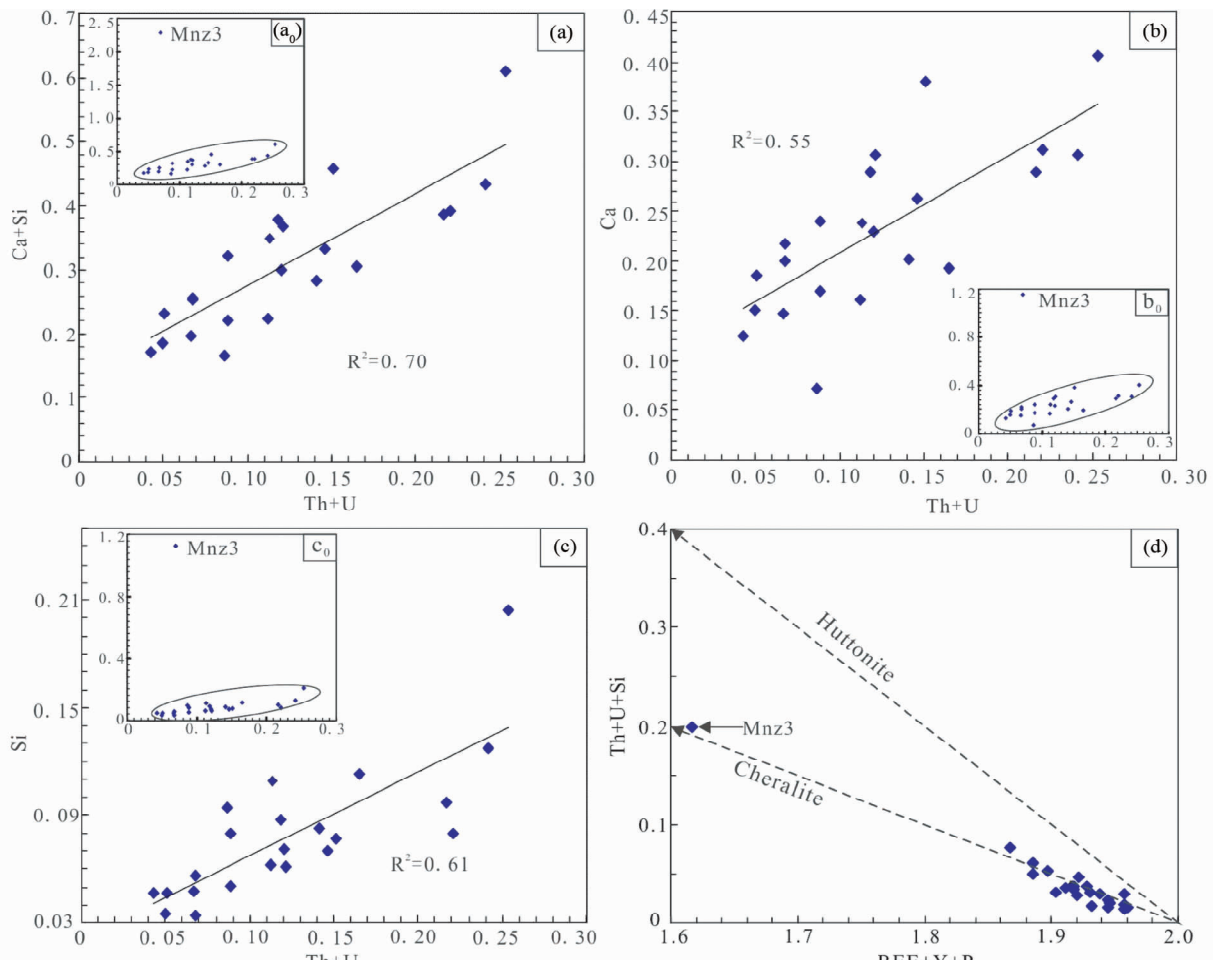


图5 独居石中组分替代图解

(a-c) Ca/Si , $\text{Ca} + \text{Si}$ 阳离子数与 $\text{Th} + \text{U}$ 阳离子数的相关性图解, 图(a-c)分别为图(a_0 - c_0)中椭圆范围内投点的局部放大; (d) $\text{Th} + \text{U} + \text{Si}$ vs. $\text{REE} + \text{Y} + \text{P}$ 图解

Fig. 5 Plots of monazite composition showing chemical replacement

(a-c) plots of Ca , Si and $\text{Ca} + \text{Si}$ vs. $\text{Th} + \text{U}$. (a-c) do not include dot 3 which is present in (a_0 - c_0); (d) plot of $\text{Th} + \text{U} + \text{Si}$ vs. $\text{REE} + \text{Y} + \text{P}$

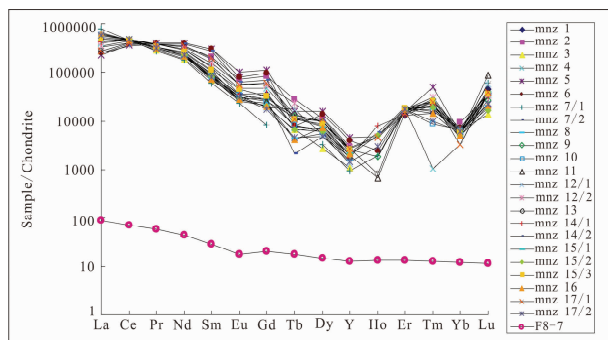


图6 独居石单矿物和透辉石透闪石岩全岩的稀土配分曲线图

全岩稀土数据来自于 Xu et al. (2014a), 球粒陨石数据来自于 Sun and McDonough (1989)

Fig. 6 The chondrite-normalized REE distribution patterns of monazites and its host rock, diopside-tremolite rock

Data for host rock from Xu et al. (2014a), data for chondrite from Sun and McDonough (1989)

$0.78\% \sim 4.61\%$, UO_2 变化范围为 $0.01\% \sim 0.05\%$, CaO 变化范围为 $0.28\% \sim 4.87\%$, PbO 变化范围为 $0.01\% \sim 0.08\%$ 。其中, ThO_2 含量明显高于低绿片岩相-低角闪岩相变质岩中的热液独居石($0\% \sim 1\%$, 大部分 $< 0.1\%$), 又区别于岩浆成因的独居石($3\% \sim 5\%$; Schandl and Gorton, 2004), 而与西格陵兰 Isua 表壳岩带的片岩和片麻岩中的独居石 ThO_2 含量比较接近(约 $1\% \sim 5\%$), 暗示了其变质成因。由分析结果可知:除测点3外,其余独居石中的 Ca 、 Si 、 $\text{Ca} + \text{Si}$ 阳离子数均与 $\text{Th} + \text{U}$ 阳离子数变化呈良好的正相关性(图 5a-c), 相应的替代关系为: $\text{Th}^{4+}/\text{U}^{4+} + \text{Ca}^{2+} = 2\text{REE}^{3+}$ 、 $\text{Th}^{4+}/\text{U}^{4+} + \text{Si}^{4+} = \text{REE}^{3+} + \text{P}^{5+}$ (Zhu and O'Nions, 1999b)。测点3 明显高的 Ca 和 Si 阳离子数($\text{Ca} + \text{Si} = 2.28$, 基于 24 氧原子)可能与其呈碎片状有关(图 5a₀-c₀), 在电子探针分析过程中易于击穿从而测到了少量钙硅酸盐矿物的成分, 但也可能与独居石中的微细包裹体有关。独居石以富钍独居石(cheralite)组分为主(图 5d)。

独居石中稀土含量变化范围为 $50\% \sim 59\%$, 明显高于其赋存岩石的全岩稀土含量(130×10^{-6} ; Xu et al., 2014a)。独居石球粒陨石标准化的稀土配分形式呈轻稀土富集型($(\text{La/Yb})_N = 33.7 \sim 142$)(图 6), Eu 异常较弱($\delta\text{Eu} = 0.46 \sim 0.82$)。其中, 轻稀土分异程度变化较大, $(\text{La}/\text{Sm})_N$ 值为 $0.74 \sim 13.5$, 可分为两组, 一组 LREE 分异程度较低($(\text{La}/\text{Sm})_N = 0.74 \sim 1.56$), 另一组 LREE 分异明显($(\text{La}/\text{Sm})_N = 2.21 \sim 13.5$), 这些稀土特征与具变质成因的独居石特征相同(Rasmussen and Muhling, 2009)。样品的全岩稀土配分形式呈轻稀土略富集型($(\text{La/Yb})_N = 7$), $(\text{La}/\text{Sm})_N$ 值为 2.99 , 具弱的 Eu 负异常($\delta\text{Eu} = 0.73$)(Xu et al., 2014a)。独居石的稀土配分特征往往与围岩及其矿物相组合有关(Zhu and O'Nions, 1999a)。独居石向上翘起的重稀土特征和全

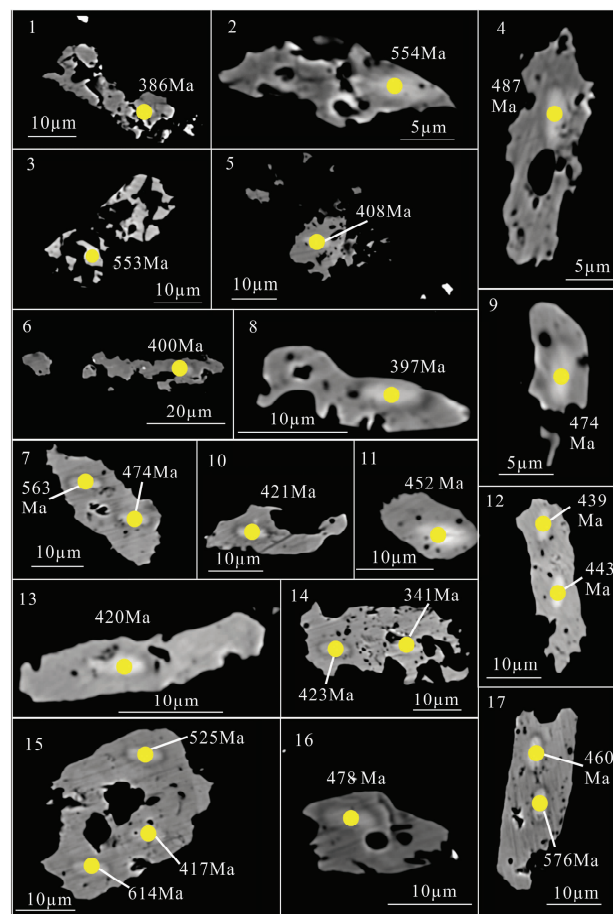


图7 独居石的电子背散射图像及分析点的表面年龄结果

Fig. 7 The back-scatter electron images for monazites marked by the apparent ages of analysis points

岩略平坦的重稀土特征均暗示了不存在石榴子石矿物相, 两者弱的 Eu 异常也表明没有斜长石矿物相产出, 这与样品中的矿物组合特征一致。

4.2 独居石年龄结果

独居石的 Th-U-Pb 年龄测试结果见表 3 和图 7。CHIME 化学定年结果表明:独居石表观年龄变化于 614Ma 和 341Ma 之间。其中, 分析点 1 和 14/2 的年龄值较低, 分别为 341Ma 和 386Ma , 可能出现了铅丢失现象, 这与两个分析点均靠近独居石颗粒溶蚀边界或裂隙的观察一致(图 7)。因此, 文中年龄意义探讨均未考虑这两个年龄。另外, 较大的表观年龄跨度可能与独居石 CHIME 化学定年本身精度有关, 如表 3 中部分年龄误差可高达 90Ma , 但独居石 CHIME 年龄仍可提供有用的变质事件信息。在本文独居石的年龄分布频谱图中(图 8a), 主峰值年龄为 455Ma , 还呈现出一个弱的 564Ma 年龄峰值。

表 3 独居石的 Th-U-Pb 化学成分结果和表观年龄

Table 3 The Th-U-Pb contents and apparent ages of monazites

测点	Th		U		Pb		Age		Th *
	(wt%)	1σ	(wt%)	1σ	(wt%)	1σ	(Ma)	±	
1	1.8043	0.0117	0.0418	0.0057	0.0350	0.0025	386	35	1.87
2	1.4504	0.0107	0.0568	0.0058	0.0429	0.0026	554	45	1.58
3	1.1849	0.0095	0.0498	0.0052	0.0325	0.0024	553	49	1.30
4	2.4112	0.0138	0.0476	0.0058	0.0588	0.0026	487	28	2.48
5	2.0005	0.0125	0.0457	0.0059	0.0450	0.0026	408	33	2.07
6	1.9426	0.0123	0.0438	0.0058	0.0420	0.0026	400	34	2.01
7/1	0.6873	0.0082	0.0298	0.0057	0.0183	0.0025	563	90	0.76
7/2	2.6738	0.0146	0.0593	0.0058	0.0628	0.0026	474	25	2.77
8	1.3780	0.0104	0.0555	0.0058	0.0279	0.0026	397	44	1.51
9	2.2689	0.0133	0.0703	0.0058	0.0557	0.0026	474	29	2.41
10	1.4052	0.0105	0.0461	0.0057	0.0299	0.0026	421	44	1.50
11	2.4336	0.0138	0.0750	0.0057	0.0561	0.0026	452	27	2.59
12/1	1.0794	0.0095	0.0301	0.0057	0.0227	0.0026	439	59	1.14
12/2	3.4938	0.0172	0.0661	0.0058	0.0781	0.0026	443	20	3.58
13	3.8432	0.0183	0.0797	0.0059	0.0818	0.0027	420	18	3.96
14/1	0.8076	0.0087	0.0202	0.0057	0.0166	0.0025	423	78	0.84
14/2	4.0507	0.0190	0.0837	0.0059	0.0703	0.0026	341	16	4.17
15/1	0.8061	0.0086	0.0161	0.0057	0.0207	0.0025	525	82	0.83
15/2	1.0675	0.0095	0.0201	0.0057	0.0316	0.0025	614	64	1.09
15/3	1.9228	0.0122	0.0403	0.0057	0.0408	0.0026	417	34	1.98
16	1.7971	0.0118	0.0612	0.0058	0.0442	0.0026	478	35	1.93
17/1	3.5609	0.0174	0.0750	0.0059	0.0826	0.0027	460	19	3.67
17/2	1.0897	0.0095	0.0283	0.0057	0.0301	0.0026	576	61	1.14

5 讨论

5.1 独居石及其球冠结构的成因

本文独居石多呈拉长透镜体状, 其长轴方向平行于赋存岩石的条纹条带(S_1 面理)及矿物线理方向, 指示了独居石为同构造变质成因(Sindern *et al.*, 2012; Williams and Jercinovic, 2002), ThO_2 含量变化(0.78% ~ 4.61%)和REE分配特征, 也暗示了独居石为变质成因。这与其赋存岩石的成因认识一致, 后者透辉石透闪石岩被认为是在区域变质和动力变质作用过程中由不纯的白云岩或含泥质的白云岩发生高达低角闪岩相变质形成的, 并叠加了后期的热液蚀变或退变质作用(许德如等, 2009; Xu *et al.*, 2014a)。

一般来说, 由于低的扩散系数(Gardés *et al.*, 2006), 独居石晶格内固态体积扩散(solid state volume diffusion)引起的化学变化在地壳 P - T 条件下可以忽略, 但受高级变质作用或岩浆长时间的影响除外(Seydoux-Guillaume *et al.*, 2004), 因此独居石常由具不同年龄的成分区组成(William *et al.*, 2007)。独居石体系的封闭温度与冷却速率和晶粒大小有关(Copeland *et al.*, 1988), 而与成分无关(Zhu *et al.*, 1997a, b)。对于粒径 $10 \sim 100\mu\text{m}$ 、冷却速率 $20^\circ\text{C}/\text{Myr}$ 的独居石颗粒来说, 其封闭温度可高达 750°C (Copeland *et al.*, 1988)。实验表明在 800°C 或更高温度时, 独居石中 U、Th、Pb 和 REE

等元素的扩散迁移速率仍较低(Gardés *et al.*, 2006), 但如果流体参与, 溶解/重沉淀或重结晶过程可使该体系在低于封闭温度条件下被完全或部分重置(Gardés *et al.*, 2006; Williams *et al.*, 2007; Zhu and O'Nions, 1999b)。而在复杂的 P - T - t 历史中, 不同的世代或成分区域往往对应着独居石的不同生长阶段(William *et al.*, 2007), 这种不同成分区复杂的分布及其明显的界线暗示了溶解-再沉淀(dissolution-reprecipitation)是独居石蚀变的常见过程(Sindern *et al.*, 2012)。文中构成 $\sim 455\text{ Ma}$ 峰值的独居石具有变化较大的 ThO_2 (0.92% ~ 4.61%)、 PbO (0.01% ~ 0.08%) 和 CaO (0.28% ~ 1.58%) 含量范围以及 Th/U 值(24.83 ~ 52.86), 暗示了其可能受到了变质流体的影响, 而较一致的年龄范围暗示了 U-Th-Pb 体系的重置。相关实验表明碱性流体可以造成独居石蚀变区中的 Pb 发生完全丢失, 从而使 U-Pb 体系重置(Harlov *et al.*, 2011; Sindern *et al.*, 2012)。另外, 构成 $\sim 564\text{ Ma}$ 峰值的独居石具有变化较小的 ThO_2 (0.78% ~ 1.65%)、 PbO (0.02% ~ 0.04%) 和 CaO (0.50% ~ 0.97%) 含量范围以及高的 Th/U 值(23.06 ~ 53.11)特征, 暗示了其是在剪切变形早阶段形成的。结合独居石沿面理方向定向分布的产出特征, 暗示了伴随剪切变形过程独居石在低角闪岩相条件下发生了溶解-再沉淀, 并在碱性的变质流体诱导下, 引起了 U-Pb 体系的局部重置, 从而形成补丁状成分区(patchy zonation)。具有 $\sim 564\text{ Ma}$ 和 455 Ma 峰值年龄的不同

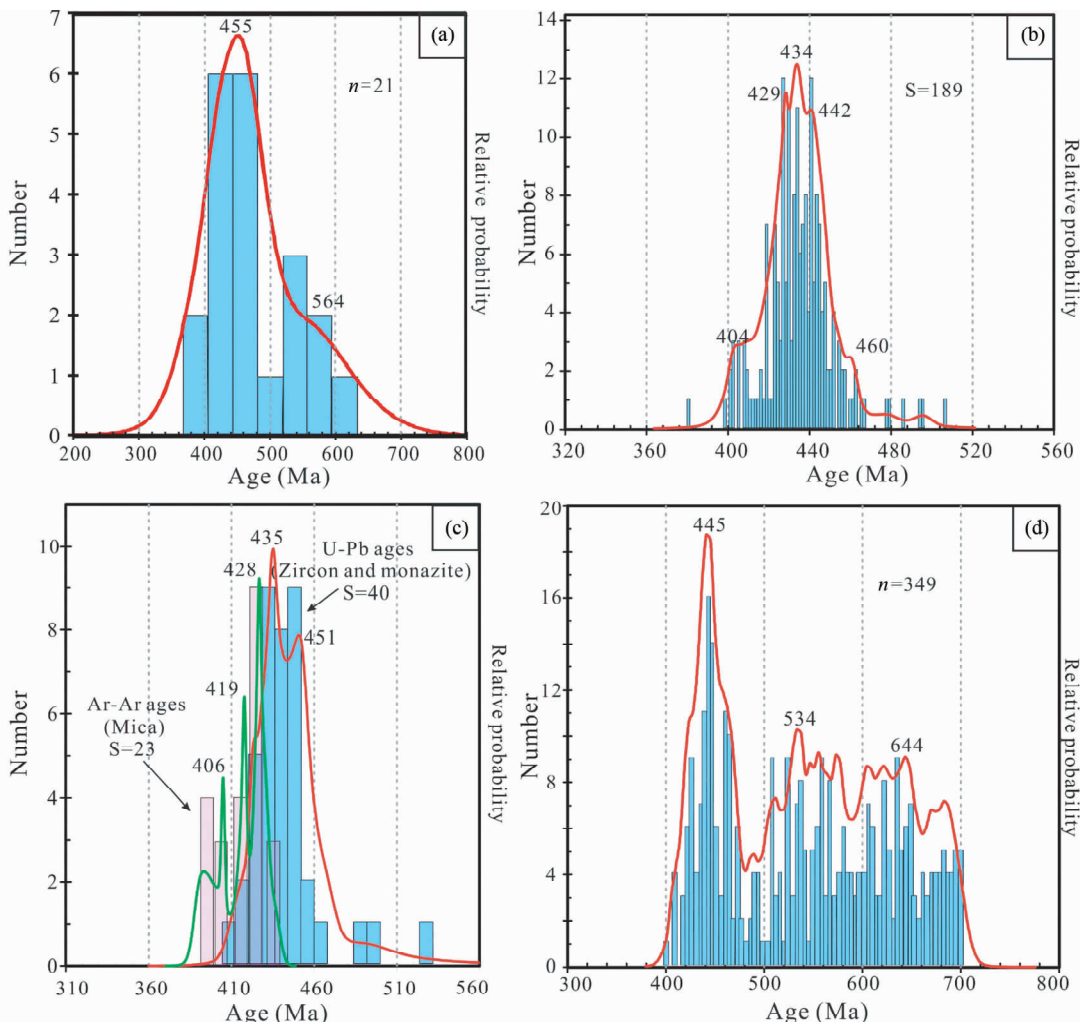


图8 年龄分布谱图

(a) 海南石碌矿区透辉石透闪石岩中的独居石年龄分布谱图,本文数据;(b) 华南加里东期岩浆作用年龄频谱图,数据主要来自 Hu *et al.* (2008), Li (1994), Li *et al.* (2010), Liu *et al.* (2010), Roger *et al.* (2000), Wan *et al.* (2010), Wang *et al.* (2007, 2011, 2013), Xu *et al.* (2005, 2011, 2014b), Yan *et al.* (2006), Zhang *et al.* (2012) 及其文中参考文献;(c) 华南加里东期变质和变形作用年龄频谱图,数据来自 Charvet *et al.* (2010), Faure *et al.* (2009), Li *et al.* (2010), Liu *et al.* (2010), Wan *et al.* (2007, 2010), Wang *et al.* (2007, 2011, 2012, 2013), Xu *et al.* (2011), Yu *et al.* (2005), 舒良树等(2008)及其文中参考文献;(d) 华南晚新元古代-古生代地层和沉积物中碎屑锆石的年龄频谱图(<700 Ma),数据来自 Duan *et al.* (2011), Wang *et al.* (2010), Wu *et al.* (2010), Xu *et al.* (2005, 2012), Yao *et al.* (2011), Yu *et al.* (2008), 向磊和舒良树(2010)及其文中参考文献. n = 碎屑锆石测点数,S = 样品数,所有锆石年龄只考虑了不一致性 $\leq 10\%$ 的数据

Fig. 8 Accumulative probability plots

(a) accumulative probability plots of monazites from diopside-tremolite rock in Shilu mining, Hainan Island, data from this text; (b) accumulative probability plots for Caledonian magmatism in South China, data from Hu *et al.* (2008), Li (1994), Li *et al.* (2010), Liu *et al.* (2010), Roger *et al.* (2000), Wan *et al.* (2010), Wang *et al.* (2007, 2011, 2013), Xu *et al.* (2005, 2011, 2014b), Yan *et al.* (2006), Zhang *et al.* (2012) and references therein; (c) probability plots for Caledonian metamorphism and deformation in South China, data from Charvet *et al.* (2010), Faure *et al.* (2009), Li *et al.* (2010), Liu *et al.* (2010), Wan *et al.* (2007, 2010), Wang *et al.* (2007, 2011, 2012, 2013), Xu *et al.* (2011), Yu *et al.* (2005), Shu *et al.* (2008) and references therein; (d) probability plots for detrital zircons from Late Neoproterozoic-Paleozoic stora and sediments (<700 Ma) in South China, data from Duan *et al.* (2011), Wang *et al.* (2010), Wu *et al.* (2010), Xu *et al.* (2005, 2012), Yao *et al.* (2011), Yu *et al.* (2008), Xiang and Shu (2010) and and references therein. n = the numbers of analytical points for detrital zircons, S = the numbers of samples, only data with $\leq 10\%$ discordance was considered

成分区分别对应于剪切变形的早、晚两个阶段。

关于独居石在变质作用过程中的稳定性和分解反应,随着电子探针技术的发展,国内外相关报道逐渐增多。球冠结

构(磷灰石+褐帘石+绿帘石)多被认为是独居石在变质条件下分解的典型特征,该现象在 Alps、Carpathians、东 Bohemian 地块以及 Taratash 杂岩体中经历了高达角闪岩相

变质作用的 S 型和高钾 I 型变质花岗闪长岩和花岗片麻岩以及变沉积岩中普遍出现 (Finger *et al.*, 1998; Rasmussen and Muhling, 2009; Sindern *et al.*, 2012)。此外,在角闪岩相变质作用及流体的条件下,十字石片岩中的独居石-绿帘石发生反应往往形成一系列富集 LREE 的矿物,相关反应式为 1.8 独居石 + 1.5 绿帘石 + 11.1H₂O + 6Fe_{aq} = 0.6 磷灰石 + 1.5 绿泥石 + 1.8REE_{aq} + 11.1H + 钉石 (Grapes *et al.*, 2005)。我国东海超高压榴辉岩中同样存在着绿帘石、褐帘石、磷灰石和钉石矿物集合体组合,其中褐帘石、磷灰石和钉石被认为是绿帘石与可能已消耗完全的独居石在超高压变质条件下的产物(王汝成等, 2006)。因此,独居石的分解反应在绿片岩相-麻粒岩相变质作用过程均可发生,其往往分解形成(钉石 ± 绿泥石)-磷灰石-褐帘石-斜黝帘石/绿帘石的矿物组合(Finger *et al.*, 1998; Grapes *et al.*, 2005; Lanzirotti and Hanson, 1996)。这种分解反应可能与温度-压力条件的变化、全岩成分、矿物-流体相互作用有关(Grapes *et al.*, 2005)。

本文球冠结构中磷灰石紧靠近独居石,且呈港湾状与独居石接触,说明磷灰石是直接交代独居石的产物。褐帘石环绕磷灰石分布且具有朝绿帘石的突刺结构暗示了褐帘石稍晚于磷灰石形成。绿帘石的半自形-它形结晶形态和多分布在球冠的最边部可能指示了绿帘石形成最晚。另外,褐帘石和磷灰石分布区的大小往往成正比,这种同心生长环带暗示了反应过程中化学计量起着重要作用,该过程不是纯的交代反应,可能由独居石到球冠矿物间的元素扩散动力学机制控制(Finger *et al.*, 1998)。详细的岩相学观察还发现,该分解反应往往发生在位于矿物边界和解理面附近的独居石周围,暗示了变质流体相及其成分对独居石的分解反应起着重要作用(Sindern *et al.*, 2012)。相关实验表明富 Ca 的流体有利于独居石的分解以及氟磷灰石和褐帘石或含 REE 绿帘石的形成;低 Ca 高 Na 的流体会降低独居石的溶解度,但有助于褐帘石的形成;低 Ca 高 K 的流体有利于具有铈磷灰石组分的氟磷灰石形成,几乎不形成褐帘石和含 REE 绿帘石;而含 NaCl 和 KCl 卤水对独居石的影响甚小,不会或仅发生弱的反应;Na₂Si₂O₅ + H₂O 流体相会使独居石发生较强的分解从而形成氟磷灰石-铈磷灰石和突厥斯坦石(Budzyn *et al.*, 2011; Harlov *et al.*, 2011; Sindern *et al.*, 2012)。另外,这些球冠尚未发生变形,证实其形成晚于岩石的剪切变形。因此,本文环状球冠物磷灰石-褐帘石-绿帘石的形成被认为发生在构造变形后,由独居石在富钙的变质流体参与条件下经绿片岩相变质作用形成的,其中磷灰石形成的反应式为 3(REE)PO₄ + 5Ca_{aq}²⁺ + H₂O → Ca₅(PO₄)₃(OH) + 3REE_{aq}³⁺ + H⁺, Ca 来自于富钙的流体相,可能与岩石中方解石或白云石的分解反应有关,P 来自于独居石,该反应导致 REE 被释放出来,参与了褐帘石和绿帘石的形成,从而最终形成独居石-磷灰石-褐帘石-绿帘石这一特殊矿物组合。这些退变质矿物的形成暗示了 REE、Y、Th 等元素在流体中是活动的,鉴于球

冠物环带较小,暗示了该过程没有重置 U-Pb 体系,但可能导致边部独居石的部分 Pb 丢失(Sindern *et al.*, 2012)。综上所述,石碌地区多阶段变质和/或热液历史在上述独居石的形成、蚀变和分解的演化过程中得到了充分体现。

5.2 构造意义

同构造变质成因的独居石化学定年可指示相应变形构造事件的年龄(Williams and Jercinovic, 2002)。以往研究将石碌矿区的构造变形划分为两期(D₁ 和 D₂)(Xu *et al.*, 2013),其中早期(D₁ 期)构造变形使石碌群和上覆的震旦系石灰顶组发生褶皱,形成了矿区主要控矿构造—轴向 NWW-SEE 的北一复式向斜以及矿物定向排列构成的 S₁ 面理,但关于该构造运动的时间尚缺乏合适的年代学限制。根据变质峰期年龄,本文同构造成因独居石的化学定年结果将该构造变形的时间很好地约束在约 564 ~ 455 Ma。其中,~455 Ma 的变质峰期年龄对应着华南加里东运动事件。华南加里东运动代表了扬子和华夏板块的板内碰撞作用,具有陆内造山构造属性(Wang *et al.*, 2013),在华南主要表现为:震旦系-下古生界地层的强烈褶皱与韧性剪切变形及区域性绿片岩相变质、广泛的岩浆活动和区域角度不整合(舒良树, 2006; 袁正新等, 1997)。大量的年代学数据(包括岩体、构造变形和变质作用)均表明华南加里东构造热事件主要发生在约 400 ~ 460 Ma(图 8b, c)。构造形迹上,近 EW 向的构造是华南加里东运动的一个重要产物,在广西大明山-大瑶山地区一带以及江西中-南部、黔中遵义一带(即黔中隆起)都有展布(邓新等, 2010; 杜远生和徐亚军, 2012; 吴浩若, 2000; 张芳荣, 2011),也出现在海南岛西部邦溪地区早古生代奥陶系地层中(许德如等, 2009)。石碌地区与上述一致的构造形迹以及年代学信息均暗示了石碌群褶皱变形是华南加里东运动的产物。另一个弱的 564 Ma 的年龄谱峰对应着冈瓦纳泛非事件的年龄。目前华南尚缺乏与冈瓦纳聚合事件相关的直接地质证据,华南是否参与了冈瓦纳聚合以及其在新元古代-早古生代的古地理位置还存在不同看法(Charvet, 2013; Li *et al.*, 2008a; Wang *et al.*, 2010, 2013; Wu *et al.*, 2010; Yu *et al.*, 2008)。沉积物中碎屑锆石的年龄谱峰常用来限制物源区,以判断古板块在超大陆聚合中的板块亲缘性。Wu *et al.* (2010)通过对华南晚新元古代-奥陶纪砂岩中碎屑锆石的研究,认为华南缺乏泛非事件的年代学和地质学证据,具有亲劳伦古陆的属性。然而,本文通过对华南碎屑锆石年龄数据的整理,发现存在着 680 ~ 530 Ma 的峰值(图 8d),该年龄与东冈瓦纳大陆的 Kuunga 造山带和北印度的 Bhimphedian 造山带年龄一致,暗示了华南在晚新元古代-早古生代与冈瓦纳具有亲缘性,部分沉积物物源可能来自于冈瓦纳大陆(Duan *et al.*, 2011; Wang *et al.*, 2010; Yao *et al.*, 2011; Yu *et al.*, 2008; 向磊和舒良树, 2010)。

华南加里东运动在海南岛的可能响应包括:早古生界及更老地层的强烈变形改造以及区域性绿片岩相变质作用(袁

正新等, 1997; 张业明等, 1998), 岛内泥盆系地层的缺失和可能的加里东期花岗岩浆活动等(Xu et al., 2007; 付建明和赵子杰, 1997; 张业明等, 1998)。本次独居石 CHIME 年龄结果为进一步确认加里东运动是海南岛地质演化历史中重要的构造事件提供了年代学证据。结合武夷-云开一带及海南岛约 470~530 Ma 的构造-岩浆事件年龄(Wang et al., 2007; Yu et al., 2005; 丁式江等, 2002; 丁兴等, 2005; 许德如等, 2007; 张爱梅等, 2011; 张业明等, 1999), 推测华南加里东运动可能与冈瓦纳大陆北部的聚合碰撞事件有关。华南在晚新元古代-早古生代可能位于东冈瓦纳大陆北缘的西澳大利亚和北印度之间, 加里东运动可能是东冈瓦纳大陆向北快速移动所引起的华南与澳大利亚-印度板块相互作用的结果(Charvet, 2013; Wang et al., 2010, 2013)。综上所述, 石碌地区的 ~564 Ma 记录了泛非事件在华南(至少是在海南岛)的响应, ~455 Ma 则记录了由泛非事件导致的冈瓦纳大陆聚合所引起的华夏和扬子的陆内造山事件, 即华南加里东运动。

5.3 成矿学意义

海南石碌铁矿以富赤铁矿而闻名, 然而关于该矿床的成矿过程和富集机制一直存在着不同的认识(Xu et al., 2013, 2014a; 侯威等, 2007; 许德如等, 2008; 袁奎荣等, 1977; Fang et al., 1994)。近年来的研究多表明该矿床为多因复成矿床, 铁、钴铜矿体的形成和富化是沉积作用、变质作用、构造变形及热液叠加等多地质作用过程结果(Xu et al., 2013, 2014a), 并将成矿作用过程划分为四个阶段, 即矿源层的沉积阶段(约 960~830 Ma)、褶皱变形和受变质矿床形成阶段(约 830~360 Ma)、印支-燕山早期构造叠加和改造富化阶段(约 250~210 Ma)和燕山晚期热液叠加成矿阶段(约 130~90 Ma)(Xu et al., 2013)。其中, 褶皱变形及伴随的韧性剪切与高温塑性流动对矿体有着明显的改造富化作用, 表现为: 铁、钴铜矿体主要呈层状、似层状或透镜状产出在向斜的核部或两翼向核部过渡部位; 富铁矿体、特别是钴铜矿体剪切变形构造如层内剪切褶皱、S-C 组构、无根钩状褶皱等发育, 糜棱岩化显著; 矿石矿物和脉石矿物定向性好, 其形成的 S1 面理走向多为 NW-SE 向。本文同构造成因独居石的 CHIME 年龄结果将这一成矿作用过程限定在约 560~450 Ma, 该时期加里东运动使石碌群发生褶皱变形并伴随着区域性绿片岩相和局部的低角闪岩相变质作用, 同时产生的变质流体受构造应力驱动促使铁、钴铜成矿元素进一步活化、迁移和富集, 在有利部位如向斜核部、构造面理等处富集, 最终使石碌铁矿演化成为沉积-变质改造型矿床。

综上所述, 本次独居石 CHIME 化学年龄提供了透辉石透闪石岩的变形变质信息, 约束了石碌铁矿控矿构造的形成时代, 为进一步认识石碌富铁矿的富集机制和完善矿床的成矿模式提供了年代学依据。该年龄还为深入研究海南岛的构造属性、华南加里东构造特征与运动时限提供了新资料,

对重塑华南板块在冈瓦纳大陆增生和裂解中的位置有着重要的启示意义。

6 结论

(1) 透辉石透闪石岩中的独居石化学成分为 Ce-La-Nd 磷酸盐, 具有富钍独居石端元组分。其沿岩石面理方向定向分布, 为同构造变质成因。电子探针 CHIME 法年龄结果为 614~397 Ma, 并获得了两个峰值年龄: 主峰值年龄 455 Ma 和次峰值年龄 564 Ma。

(2) 对应着 ~564 Ma 和 ~455 Ma 峰值年龄的独居石不同成分区分别形成于剪切变形的早、晚两个阶段, 其中晚阶段的成分区受到了碱性变质流体的影响, 发生了溶解-再沉淀作用, 该过程引起了 U-Pb 体系的局部完全重置。在剪切变形构造后, 独居石在富钙的流体参与条件下经绿片岩相退变质作用形成了磷灰石-褐帘石-绿帘石球粒物, 该过程可能有部分 Pb 丢失。

(3) 峰值年龄 ~455 Ma 和 ~564 Ma 分别记录了与华南加里东造山作用相关的区域变质和动力变质作用事件以及与冈瓦纳大陆聚合有关的泛非事件, 这两次造山事件可能对海南岛地质演化历史具有重要的影响。此外, 约 560~450 Ma 是石碌铁、钴铜矿改造富集的一个重要阶段。

致谢 野外工作得到了海南资源环境调查院肖勇院长和海南矿业联合有限公司陈福雄部长的帮助; 审稿人对本文提出了建设性修改意见; 在此一并感谢!

References

- Budzyñ B, Harlov DE, Williams ML and Jercinovic MJ. 2011. Experimental determination of stability relations between monazite, fluorapatite, allanite, and REE-epidote as a function of pressure, temperature, and fluid composition. *American Mineralogist*, 96 (10): 1547–1567
- Charvet J, Shu LS, Faure M, Choulet F, Wang B, Lu HF and Breton NL. 2010. Structural development of the Lower Paleozoic belt of South China: Genesis of an intracontinental orogen. *Journal of Asian Earth Sciences*, 39(4): 309–330
- Charvet J. 2013. The Neoproterozoic-Early Paleozoic tectonic evolution of the South China Block: An overview. *Journal of Asian Earth Sciences*, 74: 198–209
- Chen CH, Hsieh PS, Lee CY and Zhou HW. 2011. Two episodes of the Indosian thermal event on the South China Block: Constraints from LA-ICPMS U-Pb zircon and electron microprobe monazite ages of the Darongshan S-type granitic suite. *Gondwana Research*, 19 (4): 1008–1023
- Chen GD, Guan YW, Deng J, Hu HY and Liu TM. 1977. Preliminary discussion on ore-forming geotectonic conditions for the Shilu-type iron ore deposit in Hainan Island. *Journal of Central South University*, 7(3): 1–12 (in Chinese)
- Chen Q, Chen NS, Wang QY, Sun M, Wang XY, Li XY and Shu GM. 2006. Electron microprobe chemical ages of monazite from Qinling Group in the Qinling Orogen: Evidence for Late Pan-African metamorphism? *Chinese Science Bulletin*, 51(21): 2645–2650

- Copeland P, Parrish RR and Harrison TM. 1988. Identification of inherited radiogenic Pb in monazite and its implications for U-Pb systematics. *Nature*, 333(6175) : 760 – 763
- Deng X, Yang KG, Liu YL and She ZB. 2010. Characteristics and tectonic evolution of Qianzhong Uplift. *Earth Science Frontiers*, 17 (3) : 79 – 89 (in Chinese with English abstract)
- Ding SJ, Xu CH, Long WG, Zhou ZY and Liao ZT. 2002. Tectonic attribute and geochronology of meta-volcanic rocks, Tunchang, Hainan Island. *Acta Petrologica Sinica*, 18 (1) : 83 – 90 (in Chinese with English abstract)
- Ding X, Zhou XM and Sun T. 2005. The episodic growth of the continental crustal basement in South China: Single zircon LA-ICPMS U-Pb dating of Guzai granodiorite in Guangdong. *Geological Review*, 51(4) : 382 – 392 (in Chinese with English abstract)
- Du YS and Xu YJ. 2012. A preliminary study on Caledonian event in South China. *Geological Science and Technology Information*, 31 (5) : 43 – 49 (in Chinese with English abstract)
- Duan L, Meng QR, Zhang CL and Liu XM. 2011. Tracing the position of the South China block in Gondwana: U-Pb ages and Hf isotopes of Devonian detrital zircons. *Gondwana Research*, 19(1) : 141 – 149
- Fang Z, Xu SJ, Chen KR, Xia BD, Zhao JX and McCulloch MT. 1994. Mineralogenesis of Shilu iron ores with special reference to Sm-Nd isotope geochemical characteristics of Shilu Group bimodal volcanic rocks in Hainan Island. *Chinese Journal of Geochemistry*, 13 (3) : 223 – 235
- Faure M, Shu LS, Wang B, Charvet J, Choulet F and Monie P. 2009. Intracontinental subduction: A possible mechanism for the Early Palaeozoic Orogen of SE China. *Terra Nova*, 21(5) : 360 – 368
- Finger F, Broska I, Roberts MP and Schermaier A. 1998. Replacement of primary monazite by apatite-allanite-epidote coronas in an amphibolite facies granite gneiss from the eastern Alps. *American Mineralogist*, 83(3) : 248 – 258
- Fu JM and Zhao ZJ. 1997. The characteristics and tectonic settings of Caledonian granite in Hainan Island. *Journal of Mineralogy and Petrology*, 17(1) : 29 – 34 (in Chinese with English abstract)
- Gardés E, Jaoul O, Montel JM, Seydoux-Guillaume AM and Wirth R. 2006. Pb diffusion in monazite: An experimental study of $Pb^{2+} + Th^{4+} + 2Nd^{3+}$ interdiffusion. *Geochimica et Cosmochimica Acta*, 70 (9) : 2325 – 2336
- Ge XY. 2003. Mesozoic magmatism in Hainan Island (SEs China) and its tectonic significance: Geochronology, geochemistry and Sr-Nd isotope evidences. Ph. D. Dissertation. Guangzhou: Guangzhou Institute of Geochemistry, Chinese Academy of Sciences, 1 – 87 (in Chinese with English summary)
- Grapes R, Bucher K and Hoskin PW. 2005. Monazite-epidote reaction in amphibolite grade blackwall rocks. *European Journal of Mineralogy*, 17(4) : 553 – 566
- Harlov DE, Wirth R and Hetherington CJ. 2011. Fluid-mediated partial alteration in monazite: The role of coupled dissolution-reprecipitation in element redistribution and mass transfer. *Contributions to Mineralogy and Petrology*, 162(2) : 329 – 348
- Hou W, Chen HF and Peng GL. 1996. *Geotectonics of Hainan Island and Gold Metallogeny*. Beijing: Science Press, 1 – 229 (in Chinese)
- Hou W, Xiao Y and Chen FS. 2007. Main features of the Shilu ductile shear zone in Hainan Island and metallogeny of the “Beiyi-type” iron ore deposit. *Chinese Journal of Geology*, 42 (3) : 483 – 495 (in Chinese with English abstract)
- Hu YH, Zhou JB, Song B, Li W and Sun WD. 2008. SHRIMP zircon U-Pb dating from K-bentonite in the top of Ordovician of Wangjiawan section, Yichang, Hubei, China. *Science in China (Series D)*, 51 (4) : 493 – 498
- Janots E, Berger A, Gnos E, Whitehouse M, Lewin E and Pettke T. 2012. Constraints on fluid evolution during metamorphism from U-Th-Pb systematics in Alpine hydrothermal monazite. *Chemical Geology*, 326 – 327 : 61 – 71
- Lanzirotti A and Hanson GN. 1996. Geochronology and geochemistry of multiple generations of monazite from the Wepawaug Schist, Connecticut, USA: Implications for monazite stability in metamorphic rocks. *Contributions to Mineralogy and Petrology*, 125 (4) : 332 – 340
- Li XH. 1994. A comprehensive U-Pb, Sm-Nd, Rb-Sr and ^{40}Ar - ^{39}Ar geochronological study on Guidong granodiorite, Southeast China: Records of multiple tectonothermal events in a single pluton. *Chemical Geology*, 115(3 – 4) : 283 – 295
- Li XH, Zhou HW, Chung SL, Ding SJ, Liu Y, Lee CY, Ge WC, Zhang YM and Zhang RJ. 2002a. Geochemical and Sm-Nd isotopic characteristics of metabasites from central Hainan Island, South China and their tectonic significance. *Island Arc*, 11(3) : 193 – 205
- Li XH, Li ZX, Li WX and Wang YJ. 2006. Initiation of the Indosinian Orogeny in South China: Evidence for a Permian Magmatic Arc on Hainan Island. *The Journal of Geology*, 114(3) : 341 – 353
- Li ZX, Li XH, Zhou HW and Kinny PD. 2002b. Grenvillian continental collision in south China: New SHRIMP U-Pb zircon results and implications for the configuration of Rodinia. *Geology*, 30(2) : 163 – 166
- Li ZX, Bogdanova SV, Collins AS et al. 2008a. Assembly, configuration, and break-up history of Rodinia: A synthesis. *Precambrian Research*, 160(1 – 2) : 179 – 210
- Li ZX, Li XH, Li WX and Ding SJ. 2008b. Was Cathaysia part of Proterozoic Laurentia? New data from Hainan Island, South China. *Terra Nova*, 20(2) : 154 – 164
- Li ZX, Li XH, Wartho JA, Clark C, Li WX, Zhang CL and Bao CM. 2010. Magmatic and metamorphic events during the Early Paleozoic Wuyi-Yunkai orogeny, southeastern South China: New age constraints and pressure-temperature conditions. *Geological Society of America Bulletin*, 122(5 – 6) : 772 – 793
- Liu R, Zhou HW, Zhang L, Zhong ZQ, Zeng W, Xiang H, Jin S, Lu XQ and Li CZ. 2010. Zircon U-Pb ages and Hf isotope compositions of the Mayuan migmatite complex, NW Fujian Province, Southeast China: Constraints on the timing and nature of a regional tectonothermal event associated with the Caledonian orogeny. *Lithos*, 119(3 – 4) : 163 – 180
- Liu SW, Shu GM, Pan YM and Dang QN. 2004. Electron-microprobe dating of monazite and metamorphic age of Wutai Group, Wutai Mountains. *Geological Journal of China Universities*, 10(3) : 356 – 363 (in Chinese with English abstract)
- Metcalfe I. 1996. Gondwanaland dispersion, Asian accretion and evolution of eastern Tethys. *Australian Journal of Earth Sciences*, 43 (6) : 605 – 623
- Montel JM, Foret S, Veschambre M, Nicllet C and Provost A. 1996. Electron microprobe dating of monazite. *Chemical Geology*, 131 : 37 – 53
- Petrík I and Konečný P. 2009. Metasomatic replacement of inherited metamorphic monazite in a biotite-garnet granite from the Nízke Tatry Mountains, Western Carpathians, Slovakia: Chemical dating and evidence for disequilibrium melting. *American Mineralogist*, 94(7) : 957 – 974
- Rasmussen B and Muhling JR. 2009. Reactions destroying detrital monazite in greenschist-facies sandstones from the Witwatersrand basin, South Africa. *Chemical Geology*, 264(1 – 4) : 311 – 327
- Roger F, Leloup PH, Jolivet M, Lacassin R, Trinh PT, Brunel M and Seward D. 2000. Long and complex thermal history of the Song Chay metamorphic dome (northern Vietnam) by multi-system geochronology. *Tectonophysics*, 321(4) : 449 – 466
- Schandl ES and Gorton MP. 2004. A textural and geochemical guide to the identification of hydrothermal monazite: Criteria for selection of samples for dating epigenetic hydrothermal ore deposits. *Economic Geology*, 99(5) : 1027 – 1035
- Seydoux-Guillaume AM, Wirth R, Deutsch A and Schärer U. 2004. Microstructure of 24 ~ 1928 Ma concordant monazites: Implications for geochronology and nuclear waste deposits. *Geochimica et Cosmochimica Acta*, 68(11) : 2517 – 2527
- South China Iron-rich Scientific Team, Chinese Academy of Sciences (SCISTCAS). 1986. *Geology of Hainan Island and Geochemistry of Iron Ore Deposits in Shilu*. Beijing: Science Press, 1 – 313 (in Chinese)

- Chinese)
- Shu LS. 2006. Predevonian tectonic evolution of South China: From Cathaysian block to Caledonian Period folded orogenic Belt. *Geological Journal of China Universities*, 12 (4): 418 – 431 (in Chinese with English abstract)
- Shu LS, Yu JH, Jia D, Wang B, Shen WZ and Zhang YQ. 2008. Early Paleozoic orogenic belt in the eastern segment of South China. *Geological Bulletin of China*, 27 (10): 1581 – 1593 (in Chinese with English abstract)
- Sindern S, Gerdes A, Ronkin YL, Dziggel A, Hetzel R and Schulte BA. 2012. Monazite stability, composition and geochronology as tracers of Paleoproterozoic events at the eastern margin of the East European Craton (Tarataш complex, Middle Urals). *Lithos*, 132: 82 – 97
- Sun SS and McDonough WF. 1989. Chemical and isotopic systematics of oceanic basalts: Implications for mantle composition and processes. In: Saunders AD and Norry MJ (eds.). *Magmatism in the Ocean Basins*. London: Geological Society Special Publications, 42 (1): 313 – 345
- Suzuki K, Adachi M and Tanaka T. 1991. Middle Precambrian provenance of Jurassic sandstone in the Mino Terrane, central Japan: Th-U-total Pb evidence from an electron microprobe monazite study. *Sedimentary Geology*, 75: 141 – 147
- Suzuki K and Adachi M. 1998. Denudation history of the high T/P Ryoke metamorphic belt, Southwest Japan: Constraints from CHIME monazite ages of gneisses and granitoids. *Journal of Metamorphic Geology*, 16 (1): 23 – 37
- Wan YS, Liu DY, Xu MH, Zhuang JM, Song B, Shi YR and Du LL. 2007. SHRIMP U-Pb zircon geochronology and geochemistry of metavolcanic and metasedimentary rocks in northwestern Fujian, Cathaysia block, China: Tectonic implications and the need to redefine lithostratigraphic units. *Gondwana Research*, 12 (1): 166 – 183
- Wan YS, Liu DY, Wilde SA, Cao JJ, Chen B, Dong CY, Song B and Du L. 2010. Evolution of the Yunkai Terrane, South China: Evidence from SHRIMP zircon U-Pb dating, geochemistry and Nd isotope. *Journal of Asian Earth Sciences*, 37 (2): 140 – 153
- Wang RC, Wang S, Qiu JS and Ni P. 2006. Electron-microprobe compositions and chemical dating of composite grains of epidote, allanite, apatite and Th-silicate from the Sulu UHP eclogites (CCSD main hole, Donghai, eastern China). *Acta Petrologica Sinica*, 22 (7): 1855 – 1866 (in Chinese with English abstract)
- Wang XF, Ma DQ and Jiang DH. 1991a. *Geology of Hainan Island: The 2nd, Magmatic Rock*. Beijing: Geological Publishing House, 1 – 273 (in Chinese)
- Wang XF, Ma DQ and Jiang DH. 1991b. *Geology of Hainan Island: The 3rd, Structural Geology*. Beijing: Geological Publishing House, 1 – 139 (in Chinese)
- Wang XF, Ma DQ and Jiang DH. 1991c. *Geology of Hainan Island: The 1st, Stratum and Paleontology*. Beijing: Geological Publishing House, 1 – 281 (in Chinese)
- Wang YJ, Fan WM, Zhao GC, Ji SC and Peng TP. 2007. Zircon U-Pb geochronology of gneissic rocks in the Yunkai massif and its implications on the Caledonian event in the South China Block. *Gondwana Research*, 12 (4): 404 – 416
- Wang YJ, Zhang FF, Fan WM, Zhang GW, Chen SY, Cawood PA and Zhang AM. 2010. Tectonic setting of the South China Block in the Early Paleozoic: Resolving intracontinental and ocean closure models from detrital zircon U-Pb geochronology. *Tectonics*, 29 (6): TC6020, doi:10.1029/2010TC002750
- Wang YJ, Zhang AM, Fan WM, Zhao GC, Zhang GW, Zhang YZ, Zhang FF and Li S. 2011. Kwangsian crustal anatexis within the eastern South China Block: Geochemical, zircon U-Pb geochronological and Hf isotopic fingerprints from the gneissoid granites of Wugong and Wuyi-Yunkai Domains. *Lithos*, 127 (1 – 2): 239 – 260
- Wang YJ, Wu CM, Zhang AM, Fan WM, Zhang YH, Zhang YZ, Peng TP and Yin CQ. 2012. Kwangsian and Indosinian reworking of the eastern South China Block: Constraints on zircon U-Pb geochronology and metamorphism of amphibolites and granulites. *Lithos*, 150: 227 – 242
- Wang YJ, Fan WM, Zhang GW and Zhang YH. 2013. Phanerozoic tectonics of the South China Block: Key observations and controversies. *Gondwana Research*, 23 (4): 1273 – 1305
- Wang ZL, Xu DR, Zhang YQ, Chen FX, Wang L and Wu J. 2011. Zircon LA-ICP-MS U-Pb dating of the granodiorite porphyry from Shili iron ore deposit, Hainan Province and its geological implication. *Geotectonica et Metallogenesis*, 35 (2): 292 – 299 (in Chinese with English abstract)
- Williams ML and Jercinovic MJ. 2002. Microprobe monazite geochronology: Putting absolute time into microstructural analysis. *Journal of Structural Geology*, 24 (6 – 7): 1013 – 1028
- Williams ML, Jercinovic MJ and Hetherington CJ. 2007. Microprobe monazite geochronology: Understanding geologic processes by integrating composition and chronology. *Annual Review of Earth and Planetary Sciences*, 35 (1): 137 – 175
- Wu HR. 2000. A discussion on the tectonic Palaeogeography related to the Caledonian Movement in Guangxi. *Journal of Palaeogeography*, 2 (1): 70 – 76 (in Chinese with English abstract)
- Wu L, Jia D, Li HB, Deng F and Li YQ. 2010. Provenance of detrital zircons from the Late Neoproterozoic to Ordovician sandstones of South China: Implications for its continental affinity. *Geological Magazine*, 147 (6): 974 – 980
- Xiang L and Shu LS. 2010. Pre-Devonian tectonic evolution of the eastern South China Block: Geochronological evidence from detrital zircons. *Science China: Earth Sciences*, 53 (10): 1427 – 1444
- Xu DR, Chen GH, Xia B and Chen T. 2003. Comment on several important basic geological problems in Hainan Island, China. *Geological Science and Technology Information*, 22 (4): 37 – 44 (in Chinese with English abstract)
- Xu DR, Xia B, Li PC, Chen GH, Ma C and Zhang YQ. 2007. Protolith natures and U-Pb sensitive high mass-resolution ion microprobe (SHRIMP) zircon ages of the metabasites in Hainan Island, South China: Implications for geodynamic evolution since the Late Precambrian. *Island Arc*, 16 (4): 575 – 597
- Xu DR, Ma C, Li PC, Xia B and Zhang YQ. 2007. U-Pb SHRIMP-dating of zircon domains from metaclastic sedimentary rocks in Hainan Island, South China, and its geological significance. *Acta Geologica Sinica*, 81 (3): 381 – 393 (in Chinese with English abstract)
- Xu DR, Wang L, Xiao Y, Liu CL, Fu QJ, Cai ZR and Huang JR. 2008. A preliminary discussion on metallogenetic model for Shili-type iron oxide-copper-gold-cobalt ore deposit. *Mineral Deposits*, 27 (6): 681 – 694 (in Chinese with English abstract)
- Xu DR, Xiao Y, Xia B, Cai RJ, Hou W, Wang L, Liu CL and Zhao B. 2009. Metallogenetic Model and Ore Predication of the Shili Iron Ore Deposit in Hainan Province. Beijing: Geological Publishing House, 1 – 331 (in Chinese)
- Xu DR, Wang ZL, Cai JX, Wu CJ, Bakun-Czubarow N, Wang L, Chen HY, Baker MJ and Kusiak MA. 2013. Geological characteristics and metallogenesis of the Shili Fe-ore deposit in Hainan Province, South China. *Ore Geology Reviews*, 53: 318 – 342
- Xu DR, Wang ZL, Chen HY, Hollings P, Jansen NH, Zhang ZC and Wu CJ. 2014a. Petrography and geochemistry of the Shili Fe-Co-Cu ore district, South China: Implications for the origin of a Neoproterozoic BIF system. *Ore Geology Reviews*, 57: 322 – 350
- Xu XB, Zhang YQ, Shu LS and Jia D. 2011. LA-ICP-MS U-Pb and ⁴⁰Ar/³⁹Ar geochronology of the sheared metamorphic rocks in the Wuyishan: Constraints on the timing of Early Paleozoic and Early Mesozoic tectono-thermal events in SE China. *Tectonophysics*, 501 (1 – 4): 71 – 86
- Xu XS, O'Reilly SY, Griffin WL, Deng P and Pearson NJ. 2005. Relict Proterozoic basement in the Nanling Mountains (SE China) and its tectonothermal overprinting. *Tectonics*, 24 (2): TC2003, doi: 10.1029/2004TC001652
- Xu YH, Sun QQ, Cai GQ, Yin XJ and Chen J. 2014b. The U-Pb ages and Hf isotopes of detrital zircons from Hainan Island, South China:

- Implications for sediment provenance and the crustal evolution. *Environmental Earth Sciences*, 71(4): 1619–1628
- Xu YJ, Du YS, Cawood PA, Zhu YH, Li WC and Yu WC. 2012. Detrital zircon provenance of Upper Ordovician and Silurian strata in the northeastern Yangtze Block: Response to orogenesis in South China. *Sedimentary Geology*, 267–268: 63–72
- Yan DP, Zhou MF, Wang CY and Xia B. 2006. Structural and geochronological constraints on the tectonic evolution of the Dulong-Song Chay tectonic dome in Yunnan Province, SW China. *Journal of Asian Earth Sciences*, 28(4): 332–353
- Yao JL, Shu LS and Santosh M. 2011. Detrital zircon U-Pb geochronology, Hf-isotopes and geochemistry: New clues for the Precambrian crustal evolution of Cathaysia Block, South China. *Gondwana Research*, 20(2): 553–567
- Yu JH, Zhou XM, O'Reilly YS, Zhao L, Griffin WL, Wang RC, Wang LJ and Chen XM. 2005. Formation history and protolith characteristics of granulite facies metamorphic rock in Central Cathaysia deduced from U-Pb and Lu-Hf isotopic studies of single zircon grains. *Chinese Science Bulletin*, 50(18): 2080–2089
- Yu JH, O'Reilly SY, Wang LJ, Griffin WL, Zhang M, Wang RC, Jiang SY and Shu L. 2008. Where was South China in the Rodinia supercontinent? Evidence from U-Pb geochronology and Hf isotopes of detrital zircons. *Precambrian Research*, 164(1–2): 1–15
- Yuan KR, Hou GH, Li GS and Liang JC. 1977. The genesis on Shilu iron ore deposit in Hainan Province and the relations between iron-rich ores and structure. *Journal of Central South University*, (3): 26–43 (in Chinese)
- Yuan ZX, Zhong GF, Xie YB and Yu JN. 1997. A new recognition on spacio-temporal characteristics of the Caledonian orogeny happened in South China. *Geology and Mineral Resources of South China*, (4): 19–25 (in Chinese with English abstract)
- Zhang AM, Wang YJ, Fan WM, Zhang FF and Zhang YZ. 2011. LA-ICPMS zircon U-Pb geochronology and Hf isotopic composition of the Taoxi migmatite (Wuping): Constrains on the formation age of the Taoxi Complex and the Yu'nanian event. *Geotectonica et Metallogenesis*, 35(1): 64–72 (in Chinese with English abstract)
- Zhang FF, Wang YJ, Zhang AM, Fan WM, Zhang YZ and Zi JW. 2012. Geochronological and geochemical constraints on the petrogenesis of Middle Paleozoic (Kwangssian) massive granites in the eastern South China Block. *Lithos*, 150: 188–208
- Zhang FR. 2011. The geological and geochemical characteristics and its petrogenesis for Caledonian granites in the central-southern Jiangxi Province. Ph. D. Dissertation. Nanjing: Nanjing University, 1–115 (in Chinese with English summary)
- Zhang RJ, Feng SN, Xu GH, Yang DL, Yan DP, Li ZH, Jiang DH and Wu W. 1990. Discovery of Chuarria-Tawuia assemblage in Shilu Group, Hainan Island and its significance. *Science in China (Series B)*, 33(2): 211–220
- Zhang RJ, Ma GG, Feng SN and Yan DP. 1992. Sm-Nd age of the Shilu iron ore deposits on Hainan Island and its significance. *Scientia Geologica Sinica*, (1): 38–43 (in Chinese with English abstract)
- Zhang RJ, Wang CY, Hu N and Feng SN. 2001. Biostratigraphy of Famennian in Hainan Island, South China. *Science in China (Series D)*, 44(12): 1057–1064
- Zhang YM, Xu AW, Fu JM, Zhao ZJ, Wu GJ and Zeng BF. 1998. Some important fundamental geological problems in Hainan Island. *Geological Review*, 44(6): 568–575 (in Chinese with English abstract)
- Zhang YM, Zhang RJ, Hu N, Zhang SH and Duan QF. 1999. High grade metamorphic complexes in middle Hainan Island: Ages of the Pb-Pb single zircons and their geological significance. *Acta Geoscientia Sinica*, 20(3): 284–288 (in Chinese with English abstract)
- Zhu XK, O'Nions RK, Belshaw NS and Gibb AJ. 1997a. Significance of in situ SIMS chronometry of zoned monazite from the Lewisian granulites, Northwest Scotland. *Chemical Geology*, 135(1–2): 35–53
- Zhu XK, O'Nions RK, Belshaw NS and Gibb AJ. 1997b. Lewisian crustal history from in situ SIMS mineral chronometry and related metamorphic textures. *Chemical Geology*, 136(3): 205–218
- Zhu XK and O'Nions RK. 1999a. Monazite chemical composition: Some implications for monazite geochronology. *Contributions to Mineralogy and Petrology*, 137(4): 351–363
- Zhu XK and O'Nions RK. 1999b. Zonation of monazite in metamorphic rocks and its implications for high temperature thermochronology: A case study from the Lewisian terrain. *Earth and Planetary Science Letters*, 171(2): 209–220
- ## 附中文参考文献
- 陈国达, 关尹文, 邓景, 胡火炎, 柳天树. 1977. 海南岛石碌式铁矿的大地构造成矿条件初探. *中南矿冶学院学报*, 7(3): 1–12
- 邓新, 杨坤光, 刘彦良, 余振兵. 2010. 黔中隆起性质及其构造演化. *地学前缘*, 17(3): 79–89
- 丁式江, 许长海, 龙文国, 周祖翼, 廖宗廷. 2002. 海南屯昌变火山岩构造属性及其年代学研究. *岩石学报*, 18(1): 83–90
- 丁兴, 周新民, 孙涛. 2005. 华南陆壳基底的幕式生长——来自广东古寨花岗闪长岩中锆石 LA-ICPMS 定年的信息. *地质论评*, 51(4): 382–392
- 杜远生, 徐亚军. 2012. 华南加里东运动初探. *地质科技情报*, 31(5): 43–49
- 付建明, 赵子杰. 1997. 海南岛加里东期花岗岩的特征及构造环境分析. *矿物岩石*, 17(1): 29–34
- 葛小月. 2003. 海南岛中生代岩浆作用及其构造意义——年代学、地球化学及 Sr-Nd 同位素证据. *博士学位论文*. 广州: 中国科学院广州地球化学研究所, 1–87
- 侯威, 陈惠芳, 彭格林. 1996. 海南岛大地构造与金成矿学. 北京: 科学出版社, 1–229
- 侯威, 肖勇, 陈翻身. 2007. 海南岛石碌韧性剪切带的主要特征与“北一”式铁矿的成因. *地质科学*, 42(3): 483–495
- 刘树文, 舒桂明, 潘元明, 党青宁. 2004. 电子探针独居石定年法及五台群的变质时代. *高校地质学报*, 10(3): 356–363
- 舒良树. 2006. 华南前泥盆纪构造演化: 从华夏地块到加里东期造山带. *高校地质学报*, 12(4): 418–431
- 舒良树, 于津海, 贾东, 王博, 沈渭洲, 张岳桥. 2008. 华南东段早古生代造山带研究. *地质通报*, 27(10): 1581–1593
- 王汝成, 王硕, 邱检生, 倪培. 2006. 东海超高压榴辉岩中绿帘石、褐帘石、磷灰石和钛石集合体的电子探针成分和化学定年研究. *岩石学报*, 22(7): 1855–1866
- 汪啸风, 马大铨, 蒋大海. 1991a. 海南岛地质(二)岩浆岩. 北京: 地质出版社, 1–273
- 汪啸风, 马大铨, 蒋大海. 1991b. 海南岛地质(三)构造地质. 北京: 地质出版社, 1–139
- 汪啸风, 马大铨, 蒋大海. 1991c. 海南岛地质(一)地层古生物. 北京: 地质出版社, 1–281
- 王智琳, 许德如, 张玉泉, 陈福雄, 王力, 吴俊. 2011. 海南石碌铁矿床花岗闪长斑岩的锆石 LA-ICP-MS U-Pb 定年及地质意义. 大地构造与成矿学, 35(2): 292–299
- 吴浩若. 2000. 广西加里东运动构造古地理问题. *古地理学报*, 2(1): 70–76
- 向磊, 舒良树. 2010. 华南东段前泥盆纪构造演化: 来自碎屑锆石的证据. *中国科学(D辑)*, 40(10): 1377–1388

- 许德如, 陈广浩, 夏斌, 陈涛. 2003. 海南岛几个重大基础地质问题评述. 地质科技情报, 22(4): 37–44
- 许德如, 马驰, 李鹏春, 夏斌, 张玉泉. 2007. 海南岛变碎屑沉积岩锆石 SHRIMP U-Pb 年龄及地质意义. 地质学报, 81(3): 381–393
- 许德如, 王力, 肖勇, 刘朝露, 符启基, 蔡周荣, 黄居锐. 2008. “石碌式”铁氧化物-铜(金)-钴矿床成矿模式初探. 矿床地质, 27(6): 681–694
- 许德如, 肖勇, 夏斌, 蔡仁杰, 侯威, 王力, 刘朝露, 赵斌. 2009. 海南石碌铁矿床成矿模式与找矿预测. 北京: 地质出版社, 1–331
- 袁奎荣, 候光汉, 李公时, 梁金城. 1977. 海南石碌铁矿的成因和富铁矿与构造的关系. 中南矿冶学院学报, (3): 26–43
- 袁正新, 钟国芳, 谢岩豹, 余纪能. 1997. 华南地区加里东期造山运动时空分布的新认识. 华南地质与矿产, (4): 19–25
- 张爱梅, 王岳军, 范蔚茗, 张菲菲, 张玉芝. 2011. 福建武平地区桃溪群混合岩 U-Pb 定年及其 HF 同位素组成: 对桃溪群时代及郁南运动的约束. 大地构造与成矿学, 35(1): 64–72
- 张芳荣. 2011. 江西中-南部加里东期花岗岩地质地球化学特征及其成因. 博士学位论文. 南京: 南京大学, 1–115
- 张仁杰, 马国干, 冯少南, 鄢道平. 1992. 海南石碌铁矿的 Sm-Nd 法年龄及其意义. 地质科学, (1): 38–43
- 张业明, 徐安武, 付建明, 赵子杰, 吴桂捷, 曾波夫. 1998. 海南岛几个重大基础地质问题的探讨. 地质论评, 44(6): 568–575
- 张业明, 张仁杰, 胡宁, 张树淮, 段其发. 1999. 琼中高级变质杂岩中单颗粒锆石 Pb-Pb 年龄及其地质意义. 地球学报, 20(3): 284–288
- 中国科学院华南富铁科学研究所. 1986. 海南岛地质与石碌铁矿地球化学. 北京: 科学出版社, 1–313